UCRL-50026-81-1

LLNL Underground Coal Gasification Project Quarterly Progress Report— January Through March 1981

Scientific Editor: D. U. Olness

General Editor: Wallace Clements

April 27, 1981

Lawrence Livermore National Laboratory

DISCLAIMER

UCRL-50026-81-1
Distribution Category UC-90c

LLNL Underground Coal Gasification Project Quarterly Progress Report— January Through March 1981

Scientific Editor: D. U. Olness

General Editor: Wallace Clements

Manuscript date: April 27, 1981

LAWRENCE LIVERMORE LABORATORY
University of California • Livermore, California • 94550

Available from: National Technical Information Service • U.S. Department of Commerce
5285 Port Royal Road • Springfield, VA 22161 • $6.00 per copy • (Microfiche $3.50)

CONTENTS

LLNL UNDERGROUND COAL GASIFICATION PROJECT QUARTERLY PROGRESS REPORT— JANUARY THROUGH MARCH 1981

SUMMARY

We have continued our laboratory studies of forward gasification through drilled holes in small blocks of coal, approximately 1 foot on a side. Such studies give insight into cavity growth mechanisms and particulate production. However, because of the small dimensions involved, the information these tests provide is necessarily limited to aspects of cavity growth at very early times. The natural extension of these experiments to larger blocks, perhaps 10 feet or more on a side, is now being planned. These "large block tests" will be conducted at a mine, where blocks of coal will be isolated for the experiments; the objective will be to quantify early-time cavity growth. We expect to carry out these experiments during July through November, 1981.

During this quarter the preliminary process design of the Tono No. 1 field experiment in Washington has been completed. The experimental plan and operational strategy have been developed to ensure that the injection point remains near the bottom of the coal seam and that the experiment continues at least until a period of stable operation has been reached and sustained for a time. Drilling plans are complete, and plans for instrumentation of the experiment are being prepared. Designs are completed for the data management and storage system as well as the process system, and an approximate schedule for the experiment has been developed, including cost estimates.

We have continued to develop a mathematical model for the small coal block experiments in order to further our understanding of the physical and chemical processes governing the burning of the coal and the growth of the cavity within the block. This model will be adapted, later, to larger-scale coal block experiments, and finally to full-scale field experiments. We hope to obtain scaling laws and other insights from the model. A recent development of the model has been to combine the chemical kinetic reaction rate and the mass transfer rate into a single total reaction rate. For simplicity, the model is based on the burning of pure carbon. To investigate how this unrealistic assumption may affect the results, we have been comparing the model predictions against the results of coal-block burn experiments.

Groundwater samples from wells located at distances of a few feet to several hundred feet from the gasification cavities were collected before, during, and after each of the Hoe Creek tests. During this quarter, the analysis of the groundwater contamination data pertinent to the Hoe Creek No. 3 test was completed. This is an ongoing project, and we will continue to obtain and analyze groundwater samples from these test sites.

INTRODUCTION

A major objective of the U.S. Energy Program is to develop environmentally acceptable and economically sound ways to produce energy from the nation's vast coal reserves. The Department of Energy (DOE) has sponsored a number of field projects to determine the feasibility of converting coal into a clean, efficient energy source by underground coal gasification (UCG). The basic goal of the LLNL project, as a part of DOE's UCG program, is to develop a process for producing medium-heating-value gas that can be economically upgraded to pipeline quality gas or used to produce transportation fuels such as methanol or gasoline.

A decision has been made by DOE to initiate an *in situ* coal gasification project in the State of Washington at a site in the Tono Basin owned by the Washington Water Power Company. This project will begin with several large-scale, laboratory-type gasification experiments to be done at a site where the target coal seam outcrops in a mine. These initial experiments will provide information needed for final planning of two larger field experiments to be done from the surface at locations where the target coal seam is 500 feet or more underground. One of these field experiments will link the vertically drilled injection and production wells by a horizontal hole in the coal seam, directionally drilled from the surface, while the other will link the wells by reverse combustion.

The overall program will be managed by the Laramie Energy Technology Center (LETC). Participating in the various technical aspects of the program will be LETC, LLNL, Sandia National Laboratories, the Morgantown Energy Technology Center, the Washington Irrigation and Development Company (WIDCO), Pacific Power and Light, and the State of Washington. LLNL will be responsible for the gasification phase of the project.

PRELIMINARY DESIGN OF TONO NO. 1 FIELD EXPERIMENT

INTRODUCTION

A decision has been made by the DOE to initiate an *in situ* coal gasification project in the State of Washington at a site in the Tono Basin owned by Washington Water Power Company. This site has been surveyed and partially characterized[1] by a team led by Sandia National Laboratories, Albuquerque.

The program envisioned for this project is to complete the site characterization, do a short series of large-scale laboratory-type experiments called large block tests at a site in the WIDCO mine, and carry out two field experiments. The first field experiment, Tono No. 1, will use directional drilling to link injection and production wells; the second, Tono No. 2, will use reverse combustion for linking.

The site characterization that has been done so far has adequately defined the major fault structure and the lithology of the coal and overburden material in the vicinity of the planned test. Only minimal hydrological investigation has been done (two wells). Testing of these hydrology wells showed that the Big Dirty coal seam has low permeability, about 0.025 μm^2, and the siltstone above the coal has very low permeability. Two phases of the hydrology program remain to be completed: measurements related to the process itself, and those required for the environmental permits. The additional work required will be described by Murray (draft report in preparation).

Purpose of Large Block Tests

Laboratory tests of forward[2] and reverse combustion[3] in coal blocks have given some important information to aid in our understanding of the process of cavity growth. But the cavity sizes that can be produced are limited by the size of the coal blocks that can be conveniently handled in the laboratory. This means that only cavity phenomena at very early times can be studied. We are proposing a research path to address this problem. We have chosen the name "large block tests" to indicate that the tests proposed are large enough to satisfy scaling laws, while at the same time being accessible to direct examination. These tests will be done at an

this will hold true in all coal types. Although some research in injection well design will be needed before Tono No. 2 can be done reliably, it should be scheduled as soon after Tono No. 1 as possible.

A tentative layout of the two experiments is shown in Fig. 1 for the Tono Basin site. Actual placement of the experiments will be decided after the site characterization work has been completed and the possible influence of the faults indicated in the preliminary Sandia characterization has been determined.

The main technical questions concern burn cavity growth, linking channel growth, the effects of overburden collapse, and repeatability of results. How these features of the gasification process are affected by flow rate, coal type, and linking method are questions that are still not well understood.

Some of the technical questions can be answered by a series of large block tests as described, but the major economic questions such as resource recovery, oxygen utilization efficiency, and burn width can only be answered by a successful *in situ* test that is run until the effects of roof collapse have stabilized and the future cavity growth and gas quality can be predicted with reasonable certainty.

EXPERIMENTAL PLAN FOR TONO NO. 1

There are three basic assumptions implicit in the design of this experiment. First, we assume that the injection point must remain close to the bottom of the seam throughout the entire experiment;

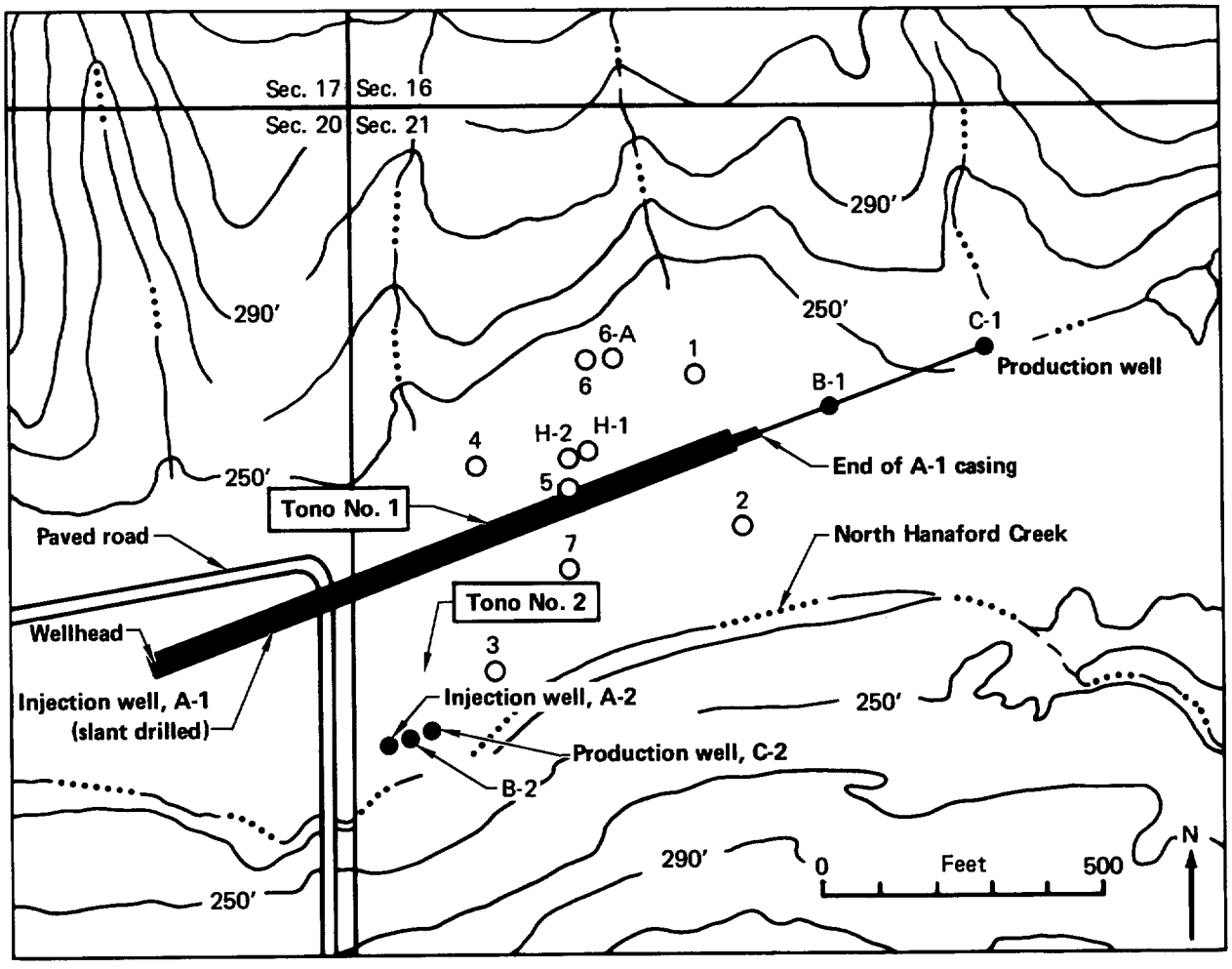

FIG. 1. Tono Basin site showing existing characterization holes and planned process wells for the Tono No. 1 and Tono No. 2 experiments.

open coal face in the open pit mine at an area that is temporarily out of production. They will allow us to directly study burn cavity growth, linking channel behavior, slag and particulate production, and many other fundamental characteristics of the *in situ* gasification process.

The tests will be of short duration, each lasting about one week, and the burn zone will be excavated afterward for visual inspection. A plan has been prepared for this project.[4] The plan covers the design, construction, operation, and evaluation of two UCG field tests whose main objective is to increase the understanding and reliability of UCG technology. A supplementary objective is to test the Tono Basin site's suitability for possible commercial gasification.

These two requirements, while compatible, do imply somewhat different approaches. For instance, a short to moderate burn time is all that is required to study initial cavity growth, but some commercially important parameters require considerably longer burn times. Because of these differences, two sets of goals are proposed for the Tono No. 1 experiment. The first set includes the basic technical goals that are essentially minimum requirements, and the second set includes supplementary goals that will significantly improve our understanding both technically and for future commercialization.

Goals of Tono No. 1

The primary goals of the experiment are as follows:

- To design the test with as ideal a geometry as is practical, so as to minimize the effects of well completion or linking techniques.
- To use oxygen-steam as the injectant in carrying out an *in situ* gasification process for a long enough time to establish a stable burn zone configuration, so that an evaluation of gas composition and oxygen utilization and an estimate of resource recovery can be made for this site.
- To monitor the performance of the burn throughout the life of the experiment.
- To determine the environmental effects of the test by monitoring groundwater contamination and earth subsidence.

Secondary goals of the Tono No. 1 experiment are:

- To carry out a test that will provide the data for an appraisal of the potential for future *in situ* gasification at this site.
- To do gas cleanup and end-use tests on a portion of the product gas stream.
- To test the throttling capability of the process for possible application to boiler start-up.
- To include a period of air burn in order to determine the usefulness of the product gas as a supplemental boiler fuel.
- To extend operating time as necessary to determine maximum burn width, maximum useful production path length, maximum subsidence effects, and long-term gas quality variations.
- To improve cavity growth diagnostics by using increased *in situ* instrumentation.

The question of product gas cleanup and possible end use testing is of interest to industry. There is a possibility that some industrial support will be made available for this kind of testing on the Tono No. 1 experiment. These tests could involve all or part of the product gas stream and would vary in complexity and cost accordingly. It is not possible to plan further for these possible aspects of the experiment without additional input from the interested parties.

One of the possible end uses for the Tono No. 1 product gas is as a start-up fuel for the coal-burning power plant boilers, to replace the diesel oil that is presently used for start-up. Such a use of the product gas implies having the capability of operating the gasifier on standby with little or no input flow for periods of time up to a week or two, then rapidly increasing flow rates for several days to start the boiler, and then shutting down again. This cyclic operational mode has been tried to a limited extent by the Russians, and in the Hanna II (Phase 1B) experiment, but not for such long shutdown periods. A simple test of this mode could be done using air injection after the primary goals have been reached.

Tono No. 1 vs Tono No. 2

Two field UCG experiments are proposed for the Tono Basin site: first an experiment with directionally drilled linking, Tono No. 1; and then an experiment with reverse combustion linking, Tono No. 2. Thus we will have a direct comparison of the results achieved by the two linking methods.

The importance of the reverse-combustion-linked experiment should not be overlooked. While the Hoe Creek No. 2[5] and Hoe Creek No. 3[6] results seem to indicate that the type of linking is not important to the process, we are not at all certain that

second, we assume that the cavity development and final burn geometry are not necessarily the same for air burns and for oxygen-steam burns; and third, we assume that we must continue the burn long enough to get well into a period of stable gas production and to get interaction with the roof material. If a stable production period is not reached, it is impossible to be sure that all of the major problems have been observed and that the results achieved are truly representative of those possible with that particular design, in that particular coal seam.

We are proposing the use of directional drilling in order to place the link channel as close to the bottom of the coal seam as possible and to extend it as far horizontally as practical, so that we can test the effectiveness and the problems associated with long underground production lines.

During the major portion of the Hoe Creek No. 2 experiment the injection point was at the bottom of the coal seam. This seam-bottom injection appeared to have a favorable influence on cavity development and quality of the gas produced. In the Hoe Creek No. 3 experiment, both injection wells were damaged, and although injection into the target Felix No. 2 coal seam was maintained for a time, a low seam injection point was not maintained. The design proposed for Tono No. 1 will allow us to test the importance of the position of the injection point for oxygen by ensuring that the injection point remains at the bottom of the seam.

Figure 2 is an elevation view showing the process well plan for Tono No. 1, and Fig. 3 is a plan view showing the process well pattern from the casing point of the directional hole to the production well. The directionally drilled hole is used as both the injection well and the linking channel. The hole is to be drilled so that it continues horizontally along the bottom of the seam—within 5 ft or less of the bottom—for 450 ft (137 m) or more if possible. The portion of the hole from the surface to the beginning of the horizontal section is to be cased and cemented, but the horizontal section is to be left uncased. The oxygen-steam lance will be inserted 50 ft (15 m) past the end of the cased portion. The uncased annulus will provide a test of a simple protective scheme for the lance and also allow for considerable horizontal growth if the lance burns off.

Assuming that we are successful in constructing the experiment as planned, it will be necessary to protect the injection system from slag

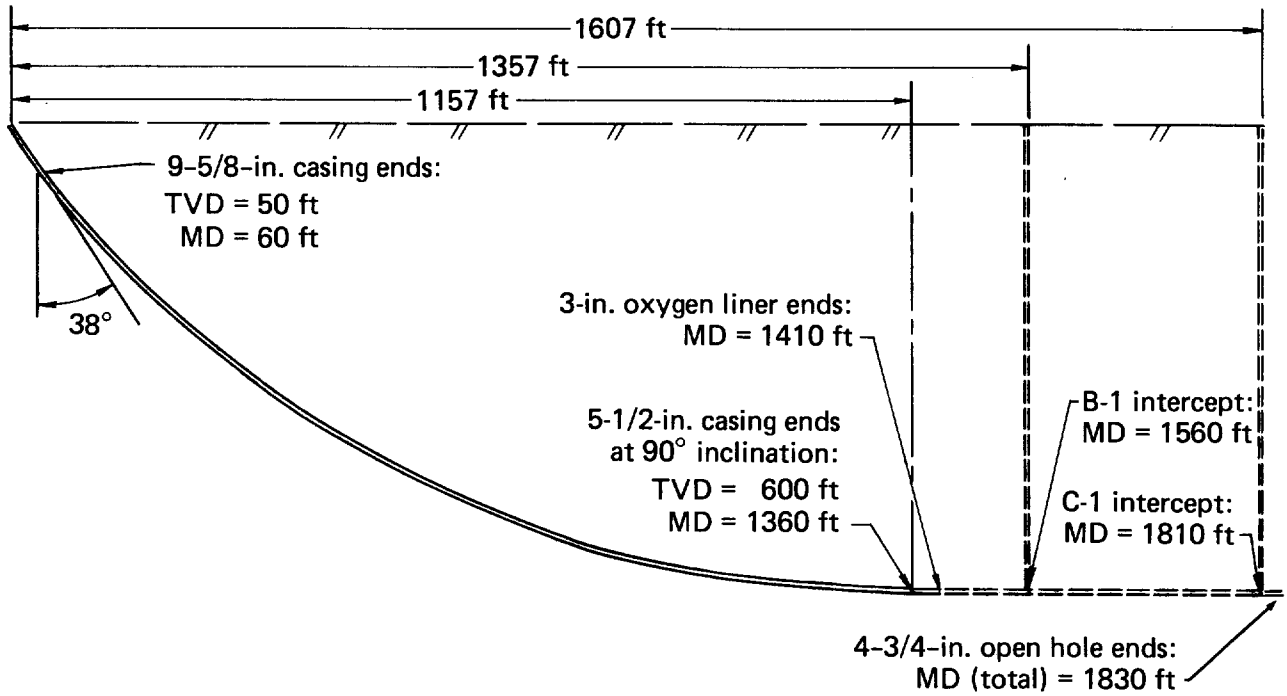

FIG. 2. Schematic vertical cross section showing the proposed path of the directionally drilled injection well for Tono No. 1. TVD = total vertical depth, MD = measured depth (i.e., length) of hole.

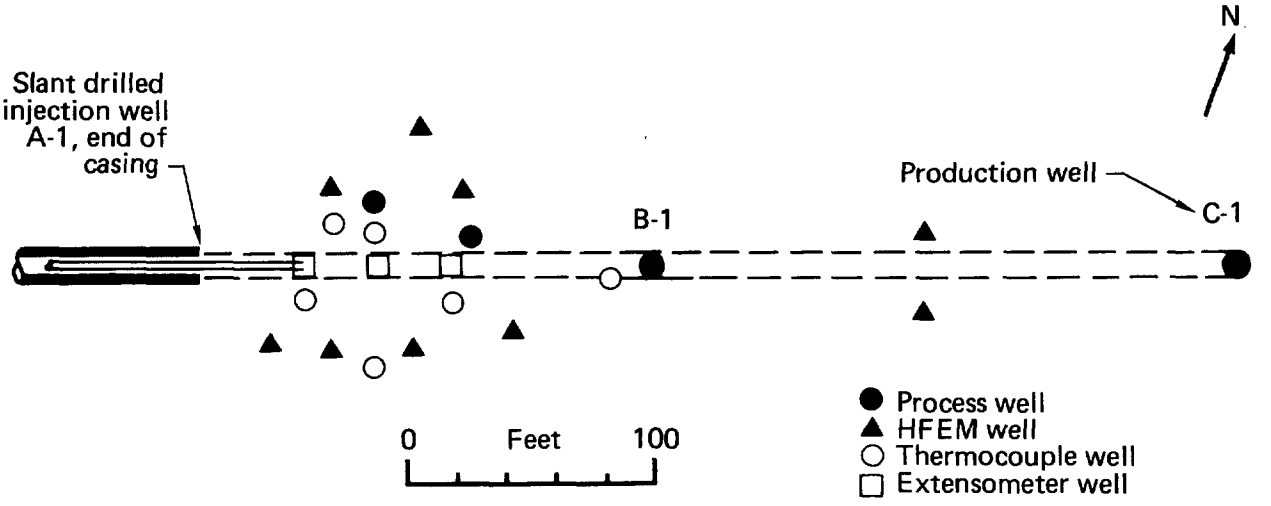

FIG. 3. Plan view of Tono No. 1 showing the process wells (A-1, B-1, and C-1) and the instrument wells. No environmental sampling wells are shown.

plugging by providing backup capability for both the oxygen and steam systems.

The choice of this particular experiment plan for Tono No. 1 is not meant to imply that we have abandoned the use of vertical injection wells. If a reliable well completion design can be developed that will survive in the very hostile oxygen burn environment, vertical wells may well be the proper choice. However, the goal for this experiment is to test the *in situ* process in the Big Dirty coal seam under the most favorable conditions, and therefore the horizontal design is preferred.

The main production well is at the end of the uncased portion of the directionally drilled hole. A production channel 400 ft (122 m) long should provide adequate protection for the well from the effects of cavity collapse and perhaps provide sufficient cooling for the gas to reduce the heat load on the production well casing. The results from Hoe Creek No. 3 indicate that the casing survived essentially intact until the end of the experiment.

The other vertical well is designed as an auxiliary injection or production well. It may or may not be used.

Having the long drilled channel increases the versatility of the experiment at little additional cost. First, of course, it gives us a test of the ability to drill long, horizontal holes close to the floor of a coal seam. Also, it provides an opportunity for achieving some of the supplemental operational goals and the possibility of determining the ultimate cavity width possible. If the channel remains more or less intact at the production end, we may be able to use the unburned portion between B-1 and C-1 at a later time for another experiment.

The oxygen-steam lance will have thermocouples fastened at intervals to provide information concerning backward cavity growth. The oxygen and steam will be mixed at the surface and injected in the central liner or lance. A small steam flow will be maintained in the annulus to prevent backward burn and to provide cooling protection for the casing and lance. Surface mixing will ensure that the injectant is well mixed when it leaves the liner and enters the burn zone.

We will use the best available logging techniques during drilling, to try to come as close as possible to intersecting the hole we are aiming at. The HFEM[7] system was used for determining hole paths after drilling at Hoe Creek with good results, and acoustic[8] and magnetic methods have been suggested for determining hole paths during drilling. If an actual intersection of holes is not achieved, the remaining separation will be linked by a method to be chosen at the time—probably by reverse combustion, with or without pneumatic fracturing. Once the two process wells, B-1 and C-1, have been linked to the directionally drilled channel, airflow tests will be done to determine the system conductance and pressure drops. Depending

on the results of these tests and on the earlier large-block surface tests, a decision will be made whether or not to enlarge the channel by reverse combustion.

If the pressure drop through the system is not excessive at the planned flow rate, we will ignite the coal in the channel at the end of the oxygen injection lance. The starting oxygen-to-steam ratio will be established by previous block tests and model calculations. The injection flow rate will be increased gradually over a period of several days, using all available diagnostics to monitor cavity growth and gasifier performance.

The primary gas production point will be well C-1; sufficient water cooling will be used to maintain the well temperatures in the 100–200°C range. Well B-1 will be used only if necessary. It will be designed to be used either for injection or production, but to change from one mode to the other we may have to shut down the experiment in order to reconfigure piping if budgetary constraints preclude dual piping systems.

The primary goals of the experiment can be achieved with a burn time of about 30 days. A longer burn time would be desirable, to satisfy some of the secondary goals, if additional funding were available.

A separate pipe, run alongside the oxygen lance, will be used for ignition of the forward burn. Although some experimentation with igniting materials will be necessary before a final choice is made, the most likely candidate is triethylborane (TEB), a pyrophoric liquid that was used successfully by ARCO and Gulf to ignite their burns.

We are designing a wire-line casing cutter which can be inserted into the injection pipe and positioned at any point along the pipe. This remotely controlled casing cutter will allow us to regain injection flow in case of plugging of the injection lance. It will also allow us to perform a test of the controlled retracting injection point (CRIP) system.[9] The CRIP gasification system is designed to minimize the effects of roof collapse by retracting the injection point by a controlled amount whenever the gas quality begins to decline. In this way the burn zone is moved back into fresh coal in a confined geometry. Efficient gasification is resumed, and the burn continues until the cavity again reaches a condition where the gas quality declines. Another retreat is made and the process starts over again. This step-by-step retraction of the injection point is continued along the entire horizontal length of the injection pipe by successive cuttings of the pipe.

The 50 ft of oxygen-steam liner in the uncased section of the horizontal hole will provide an excellent opportunity to try the CRIP method late in the burn when the other goals have been attained.

DRILLING PROGRAM

The design of the directional hole for Tono No. 1 is illustrated in Fig. 2. Conventional tooling will be used for construction and completion of this hole, thus imposing normal oil-field industrial limits on hole size, maximum turning radius, directional control, and casing point locations.

The injection well link azimuth shown in Fig. 2 corresponds to a convenient preliminary layout of the two production wells, B-1 and C-1. If follow-on site characterization data show fault lines or high permeability flows in locations inconvenient to this layout, appropriate changes to the azimuth line will be made.

The drill rig employed for this work will be a top-head-drive unit with slant drilling capability. An Ingersoll-Rand Model TH-100, TH-200, or equivalent rig will most likely be used. Tooling will include conventional drill rod and tri-cone bits as well as flush-coupled casing and downhole mud motors to accommodate directional control. Hole directional surveying tools will include magnetic single-shot (wire-line) and gyrostabilized units. A completely enclosed mud-recirculating system will be used to ensure drilling fluid control for stabilizing and cleaning the hole as drilling progresses.

We anticipate that the drilling program briefly outlined above will be accomplished in roughly two months of on-site operations. This includes all necessary mobilization and demobilization efforts, running casing, and cementing operations.

INSTRUMENTATION

The results from the Hoe Creek experiments have shown that both the high-frequency electromagnetic (HFEM) technique and standard thermocouple arrays provide useful and complementary information for burn cavity diagnostics.[10] The HFEM system is especially valuable for monitoring the burn progress down the channel and vertically

in the coal seam, because it detects all changes occurring in the plane containing the HFEM well pair. Thermocouple wells have a limited radius of sensitivity, only a few feet, and it is possible for the burn to pass between wells without detection. However, the widening of the burn cavity during the later stages of the experiment is most easily determined by thermocouples.

A combination of HFEM and thermocouple diagnostic wells seems to be the best solution, with the HFEM system dedicated to monitoring the burn progress down the channel and the thermocouples arranged to monitor lateral growth of the cavity. Both standard thermocouple strings and inverted thermocouples (Sandia Laboratories' LATRAN design[11]) will be used. Thermocouples fastened to the process wells will provide additional information; with the Tono No. 1 design, the injection well thermocouples are particularly important for observing possible backward cavity growth.

Drilling accuracy imposes a practical limit on the design of instrument well patterns. At a depth of over 600 ft, the bottom of the hole can be expected to be horizontally displaced by 3 to 6 ft with respect to the top, on the basis of standard drilling experience. Thus well patterns that depend for their effectiveness on close spacing or precise location are not advisable. The well pattern shown in Fig. 3 is intended to serve as a guide for cost analysis of the experiment. The final placement of HFEM and thermocouple wells will depend on information gathered during final site characterization, once the actual location of the directional channel is known. The high-frequency attenuation properties of the medium must be determined before the location of either the HFEM or LATRAN systems can be made final.

Three borehole extensometers are shown in Fig. 3. These instruments consist of a series of anchors embedded in the overburden at several points. The vertical motions of these anchor points are read remotely, giving a direct indication of subsurface roof collapse.

Although environmental water sampling wells could be considered part of the subsurface instrumentation, that part of the program will be described in detail in a separate document. However, coordinated planning will be necessary to ensure that the positions of the water sampling wells are compatible with the process design.

DATA ACQUISITION AND STORAGE

The process instrumentation and data acquisition systems for this experiment will be very similar to those used for the Hoe Creek No. 3 experiment, with some improvements in the computer system. The only major change anticipated is the addition of a particulate monitoring and measurement system, preferably done by outside contract.

The Tono No. 1 data acquisition and storage system will build upon the computer operating system developed for Hoe Creek No. 3. The experimental data to be collected fall into three categories:

1. Process data.
2. Compositional data.
3. Diagnostic data.

Process Data

Parameters that determine the state of operation of the aboveground facility constitute process data. They include:

- System pressures and temperatures throughout the aboveground process piping.
- Pressure, temperature, and differential pressure for each process flow-metering station.
- Parameters pertinent to process geometry—e.g., orifice size, active metering station, etc.
- Parameters pertinent to specific process equipment—e.g., boiler, compressors, incinerator, flare, etc.

Compositional Data

The flow rates of all streams entering or leaving the system will be computed from the process data. Compositional data will be collected for the product stream and the oxygen injection stream. The process-stream flow rates and compositions will be used in energy and material balances to calculate variables that cannot be measured directly, such as char accumulation and heat loss to inert materials underground.

Diagnostic Data. The state of the process underground will be monitored using diagnostic tools. These include:

- Downhole thermocouples at fixed locations in each instrument well and process well.
- HFEM probing techniques.
- Geophysical measurements.
- Tracer measurements.

The downhole thermocouples located throughout the coal seam and in the overburden contribute a large portion of our diagnostic data. Each thermocouple will be routinely measured for junction voltage, loop resistance, and resistance to ground, thus providing not only temperatures but diagnostic information concerning thermocouple failure.

Tracer techniques will be used to obtain information concerning the fluid dynamics in the system and the propagation of the burn zone through the coal seam. Two types of tracer information will be utilized during Tono No. 1: (1) helium tracers, and (2) D_2O or T_2O tracers.

A pulse of helium tracer gas will be injected periodically along with the injection stream, and the resultant response in the production stream will be measured. Continuous data will be collected, beginning with the first response and continuing to a point where little or no detectable helium remains. The data will help to provide measurements of the active volume and dispersiveness of the underground system.

The D_2O or T_2O tracer will be used to help determine the role of injected *in situ* water in the process.

The hardware components of the data acquisition and storage system fall into two categories:

1. Data acquisition hardware.
2. Data management hardware.

Data Acquisition Hardware

The bulk of the process and diagnostic data will be routinely collected by two COMUX digital voltmeter scanners, each equipped with 252 channels. The COMUX, designed by Sandia Laboratories, measures a thermocouple junction's voltage, loop resistance, and resistance to ground, all on a single channel. This feature allows complete monitoring of a thermocouple using only a single channel. The downhole thermocouples will be connected to the COMUX, as well as most of the aboveground thermocouples.

In addition to the thermocouples, several other data-gathering instruments will be directly linked to the COMUX for routine data acquisition. These include:

- Pressure transducers to measure the aboveground and downhole pressure throughout the system.
- Humidity meters to measure the water content in the produced gas and the ratio of water to organic liquid.
- Borehole extensometers to measure ground movement.

Much of the constituent data will be analyzed on-line in the field via a time-of-flight mass spectrometer analyzer and a gas chromatograph. The primary gas-sampling system will be the mass spectrometer, with sampling times as short as 10 seconds. This will provide essentially real-time analysis of the composition of the product gas. The gas chromatograph data will be collected at 60-minute intervals for backup and calibration of the mass spectrometer system.

In addition, the mass spectrometer will sample injected gas for oxygen-to-tracer ratios. During helium tests, the mass spectrometer will determine helium concentrations in the product gas as a function of time.

A liquid condenser system will provide batch backup to the humidity meter system used for water and organic content determinations. It will also provide liquid samples for field and laboratory analysis of trace elements, chemically tagged water, and organic components. All liquid condenser data will be gathered manually.

Data Management Hardware

All of the data collected by the COMUX scanner, gas chromatographs, and mass spectral analyzer will be automatically recorded at regular intervals with a Hewlett-Packard 21MX-E Computer. The primary tasks of the computer are:

1. Real-time acquisition and archiving of all relevant process data.
2. Real-time data reduction.
3. Real-time data display and retrieval.

The software for the system has as its base the Hewlett-Packard RTE IV operating system. Built on top of this base is a series of system and user programs to perform the tasks mentioned above. System programs are defined as those which perform the basic data acquisition and archival tasks, while user programs are those which perform data display and manipulation functions.

Of the three major tasks performed by the computer system, the one of highest priority is the acquisition and archiving (on magnetic tape) of all relevant process variables at regular intervals.

The second major task is to provide real-time data reduction. System programs convert all incoming analog or digital signals to useful engineering units, and user programs perform a number of heat and mass balances and pressure-drop/flow calculations useful in interpreting the performance of the gasification process.

The final major task of the system is to display the raw and reduced data on demand, showing either current values of selected variables or the time history of any variable throughout the course of the experiment.

ESTIMATING PROCESS PERFORMANCE

We have estimated process performance for the experiment using a simple gas compositional model. This model is not fully predictive in nature, but it does yield performance estimates consistent with material and energy balance constraints, and it has been used in the past to match gas composition results from the Hanna and Hoe Creek tests.[12]

The estimates we have made of process performance probably represent an upper bound on gasification efficiency, since we assumed low *in situ* heat losses (3%) and no *in situ* water influx, both of which are optimistic assumptions. However, the actual performance could turn out to be slightly better—at least with respect to gas heating value—than our estimated performance. This possibility has to do with the amount of pyrolysis gas (high in heating value) that enters the product stream. In the current estimate, the pyrolysis gas is limited in two ways. No net excess pyrolysis is allowed (i.e., all the produced char is consumed), and half the produced pyrolysis gas is recycled into the combustion-gasification zone and is consumed. It is quite possible that, in the actual test, more pyrolysis gas may enter the product stream than is allowed by these assumptions.

In making the estimates we used the full-seam coal composition shown in Table 1, obtained from the Sandia draft report on characterization of the Tono site. This analysis was then reduced to the form shown in Table 2 for use in the gas compositional model.

The results of the model calculations for two different steam/oxygen ratios are shown in Table 3. The model does not explicitly deal with the sulfur in the coal, but we have made the assumption, based on our experience at Hoe Creek, that nearly all the

TABLE 1. Composition of coal in Big Dirty seam.

	As received	Dry basis
Proximate analysis:		
Moisture (wt%)	18.42	—
Ash (wt%)	38.52	47.22
Volatile (wt%)	22.53	27.62
Fixed Carbon (wt%)	20.53	25.16
Energy content (Btu/lb)	5059	6201
Ultimate analysis:		
Moisture (wt%)	18.42	—
Carbon (wt%)	30.02	36.80
Hydrogen (wt%)	2.38	2.92
Nitrogen (wt%)	0.85	1.04
Chlorine (wt%)	0.01	0.01
Sulfur (wt%)	1.36	1.67
Ash (wt%)	38.52	47.22
Oxygen (by difference) (wt%)	8.44	10.34

TABLE 2. Coal parameters used in model to estimate process performance.

Coal composition (wt%):	
Coal (dry, ash-free)	**43.1**
Water	**18.4**
Ash	**38.5**
Pseudo coal molecule	$CH_{0.95}O_{0.21}$

sulfur in the coal seam will appear as H_2S in the product stream. Implicit in the results shown in Table 3 is the assumption of 100% gas recovery.

The energy fractions shown in the table are the fractions of the original combustion energy of the consumed coal that end up in the various categories. Since we assumed zero water influx, and since the water in the coal can be utilized in the gasification reactions, the net heat used to generate steam *in situ*, under our definitions, is zero. Also, we should point out that our estimate of the fraction of energy lost to the ash is only 0.02. This assumes that all the ash in the consumed coal remains at a temperature of 700°C. If it is found that the ash also undergoes some moderately endothermic reaction upon heating (e.g., carbonate decomposition), this heat loss number will increase and its detrimental effect on the process will increase. However, most of our concern over the high ash content centers on the fusing of the ash and the insulation of the coal by this fused ash, rather than on its impact on the total heat loss to the process.

PROCESS SYSTEM DESIGN

The process systems for the experiment will be designed to provide for: (1) introduction of injection air, steam, and oxygen into the coal seam at a controlled and measured rate; (2) removal and disposal of both gaseous and liquid products from the coal seam at measured flow rates with the added feature of providing backpressure control on the coal seam; (3) removal and disposal of formation liquids from the base of the coal seam both before and during gasification; and (4) ignition of the coal seam at the base of the production (exhaust) well to initiate the reverse-combustion linking process. A simplified schematic of the process systems designed to support the gasification test is shown in Fig. 4.

The injection system consists of piping, valving, instrumentation, and generating sources for introduction of air (which is included for use during the linking portion of the combustion process), oxygen, and steam into the injection process well.

Air Injection

The air injection system consists of diesel-driven air compressors, each rated at 200 scfm at a delivery pressure of 300 psig. These are constant-speed, constant-flow units, with limited means for controlling the discharge pressure. Compressors are normally operated at constant discharge pressure, with pressure control provided by the downstream part of the system (see Fig. 4).

The air compressors are manifolded together through separate valving so that any one or all can be used to supply the system. The common manifold is connected to injection well A through piping equipped with flow, pressure, and temperature instrumentation. Branch piping (not shown) from the injection system provides air to well B through a temporary connection to support airflow testing and for ignition of the coal seam at the base of the well. Also, branch piping leads to production well C to support airflow testing and to provide combustion air during reverse combustion linking of well C to well B. Injection airflow instrumentation to well A can be common or separate depending on the operational plan.

Instrumentation for the air injection system includes standard Chromel-Alumel thermocouples for temperature measurement, strain-gauge transducers for pressure measurement (0–450 psia), and sharp-edged orifice meters for flow measurement. Flow into well A is measured through either of two parallel orifice flow tubes. The redundancy is provided to expand the flow measurement range without changing orifice plates. Additional temperature and pressure indications are recorded from detectors located at all three wellheads.

Automatic flow control into well A or well B is provided for operators in the control room, where signals carrying uncorrected values of flow, temperature, and pressure are indicated and recorded. Pressure/temperature corrections are used to normalize gross flow measurements, which are fed into an electronic controller for error detection and adjustment to its output signal of 4–20 mA. The controller output is routed to an electronic-to-pneumatic converter which maintains the air actuator on the flow control valve in its adjusted position. The air-actuated flow control valve is specified

TABLE 3. Process performance, assuming low heat and no water influx.

	H_2O/O_2 = 2	H_2O/O_2 = 4
Coal consumption:		
(Mg)	5540	5320
(Mmol)	146	141
(m^3)	4080	3920
(tons)	6100	5860
Average injection flow (mol/s):		
Oxygen	20	20
Steam	40	80
Gasification period (days)	30	30
Total oxygen consumption:		
(Mmol)	52	52
(tons)	1830	1830
Total steam consumption:		
(Mmol)	104	207
(10^3 gal)	494	983
Product gas flow rate (mol/s)	134	170
Product gas temperature (°C)	600	600
Cooling water flow rate for gas temperature of 350°C:		
(mol/s)	20.8	27.4
(gpm)	5.9	7.8
Product-gas flow rate after cooling (mol/s)	155	197
Heat of combustion of dry, H_2S-free product gas:		
(kJ/mol)	250	230
(Btu/scf)	280	260
Heat of combustion of dry, H_2S-free product gas per mole of oxygen injected (kJ/mol)	1180	1110
Composition of dry, H_2S-free product gas (mole fractions):		
H_2	0.42	0.46
CO	0.27	0.17
CO_2	0.26	0.33
CH_4	0.05	0.04
C_2H_6	0.003	0.002
Product gas ratios (mole ratio of component to dry, H_2S-free gas):		
H_2O/gas (before cooling)	0.41	0.74
H_2O/gas (after cooling)	0.49	0.78
H_2S/gas	0.010	0.009
Total sulfur production:		
(Mg)	75	72
(tons)	83	79
Fractional distribution of consumed coal energy:		
Combustible gas	0.86	0.84
Heat loss *in situ*	0.03	0.03
Heat loss to ash	0.02	0.02
Sensible heat of product before cooling	0.09	0.12
Net *in situ* steam production	—	—

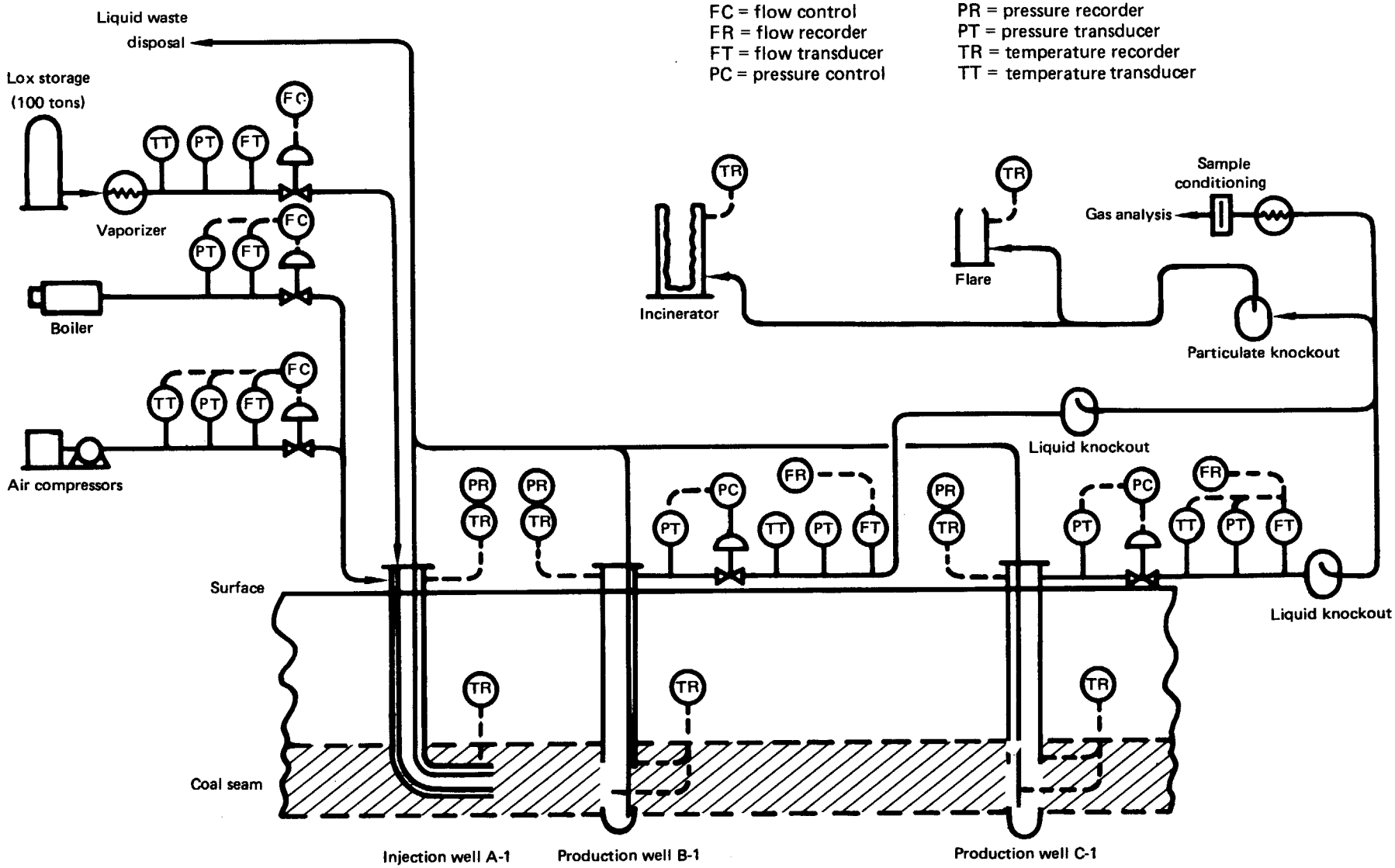

FIG. 4. Schematic diagram showing interconnection of process components for the Tono No. 1 experiment.

to provide a linear flow-to-signal output; its actuator is spring-loaded to close in the loss-of-air condition and is equipped with a mechanical manual override. (See Fig. 5.)

Oxygen Injection

Oxygen will be used as the major combustion reactant gas. The source of the oxygen will be a vendor-provided system for storing liquid oxygen and vaporizing it into gaseous form for injection into the coal seam. Liquid oxygen will be trucked to the site as required to maintain sufficient inventory. Either site-provided steam or electric power can be used to vaporize the liquid oxygen and provide the required flow rate of gaseous oxygen.

Oxygen is shown routed to injection well A through an all-stainless-steel or copper-based-alloy system. This piping will be subjected to a cleaning process including solvent degreasing before it is used to carry oxygen. Immediately upstream of well A's wellhead, instruments to measure oxygen flow, temperature, and pressure are provided. At the wellhead, the oxygen is fed to a mixing chamber to which steam is also supplied. The mixture is fed to the well through a nozzle in the top of the wellhead. The flow is conducted through a separate supply liner covering the length of well A to a point approximately 100 ft from the coal ignition point, where a transition to Monel piping is provided. The lower section of the liner and well casing are equipped with redundant thermocouples to monitor temperatures in the region of the point of oxygen-steam injection.

Instrumentation for the oxygen injection system is functionally similar to that for the air injection system. Flow measuring elements will be orifice meters with differential pressure transducers providing an output signal of 4–20 mA. Two orifice meters covering separate ranges are used to span the operating range of flows expected.

The schematic diagram shown in Fig. 5 is typical of the oxygen flow-control system with the exception of the change in flow transmitting elements. Fully automatic control of oxygen flow is available from the control room. The flow control valve is configured to close upon loss of instrument air, as in the case of the airflow control valve.

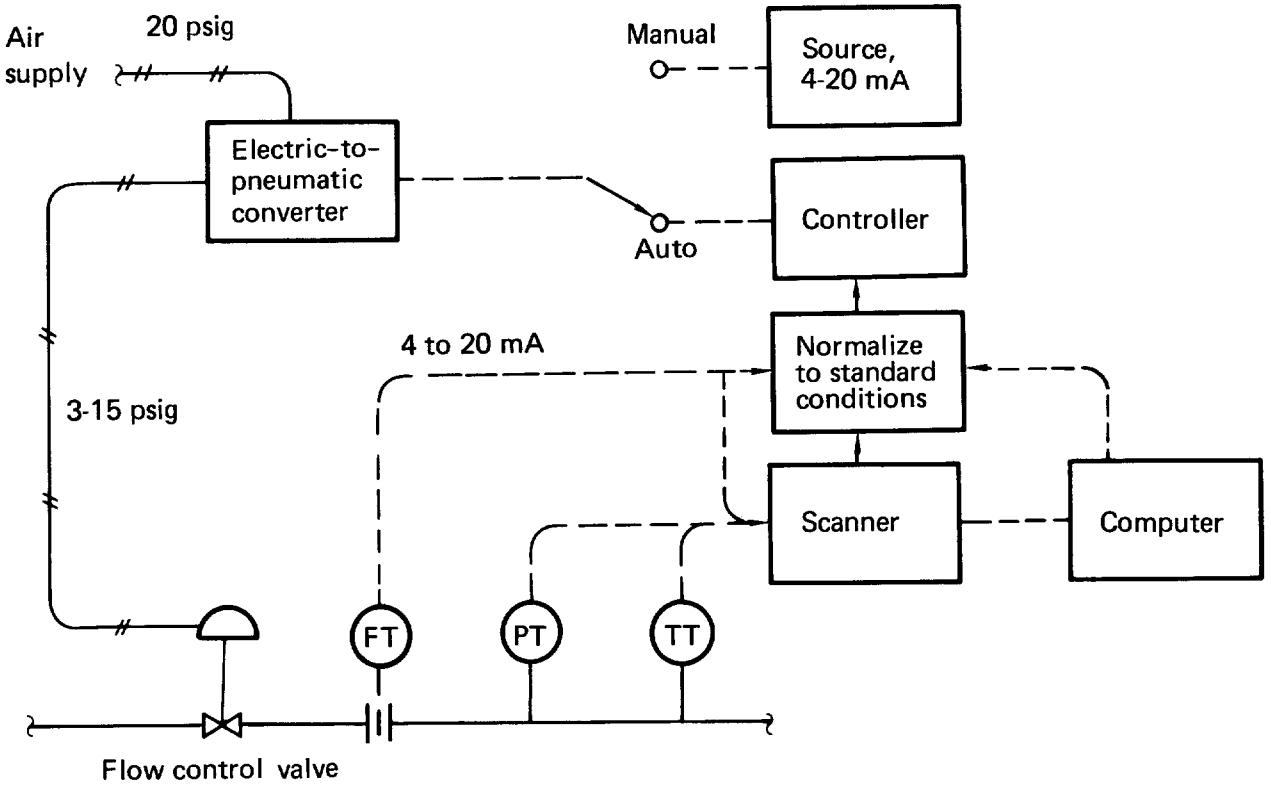

FIG. 5. Flow control system for Tono No. 1.

Steam Injection

During the steam-oxygen injection phase of the operation, steam is provided by a trailer-mounted field boiler rated at 400 bhp (boiler horsepower). This unit is equipped with integral feed-water treatment (de-aeration and water conditioning), feed-water pumps, and burner and boiler controls. The unit is capable of producing 14,000 lb/hr of saturated steam at 600 psig.

Steam is introduced into the reaction zone piping from the boiler to the steam-oxygen mixing chamber (see Fig. 4). Steam enters the coal-seam reaction zone entrained in the oxygen stream in the injection liner.

Instrumentation for the steam system is identical to that for the oxygen injection system. Two orifice meters equipped with seal pots to isolate the pressure transducers for flow detection are mounted in parallel to cover the range of expected operating requirements. (See Fig. 5.)

Exhaust Gas System

The downstream portion of the major piping system originating at the base of well B or well C comprises the exhaust system for the gas produced in the experiment. Backpressure control, flow measurement, and disposal of the product gas are the major functions of this system. A section of exhaust pipe leading from well A is provided to handle exhaust gases during coal seam ignition and to support preignition airflow testing. Well C is similarly connected through separate flow instrumentation.

The main exhaust manifold contains two parallel sections. One bypasses the pressure control valve, and the other provides redundant flow-meter sections. The discharge end of the exhaust line terminates in two product-gas disposal components: a refractory-lined incinerator at ground level, and an elevated flare. These units are operated in parallel to accommodate disposal of the expected wide variety of combustible constituents in the gas stream.

Instrumentation for the exhaust system is essentially similar to that for the injection systems. Orifice sizes are increased, and pressure transducers are lower in range (0–300 psia). Exhaust flow is recorded and normalized to standard conditions in the control room.

Automatic combustion-zone backpressure control is available for remote operation from the control room. A schematic diagram of this system is shown in Fig. 6. The wellhead discharge pressure is

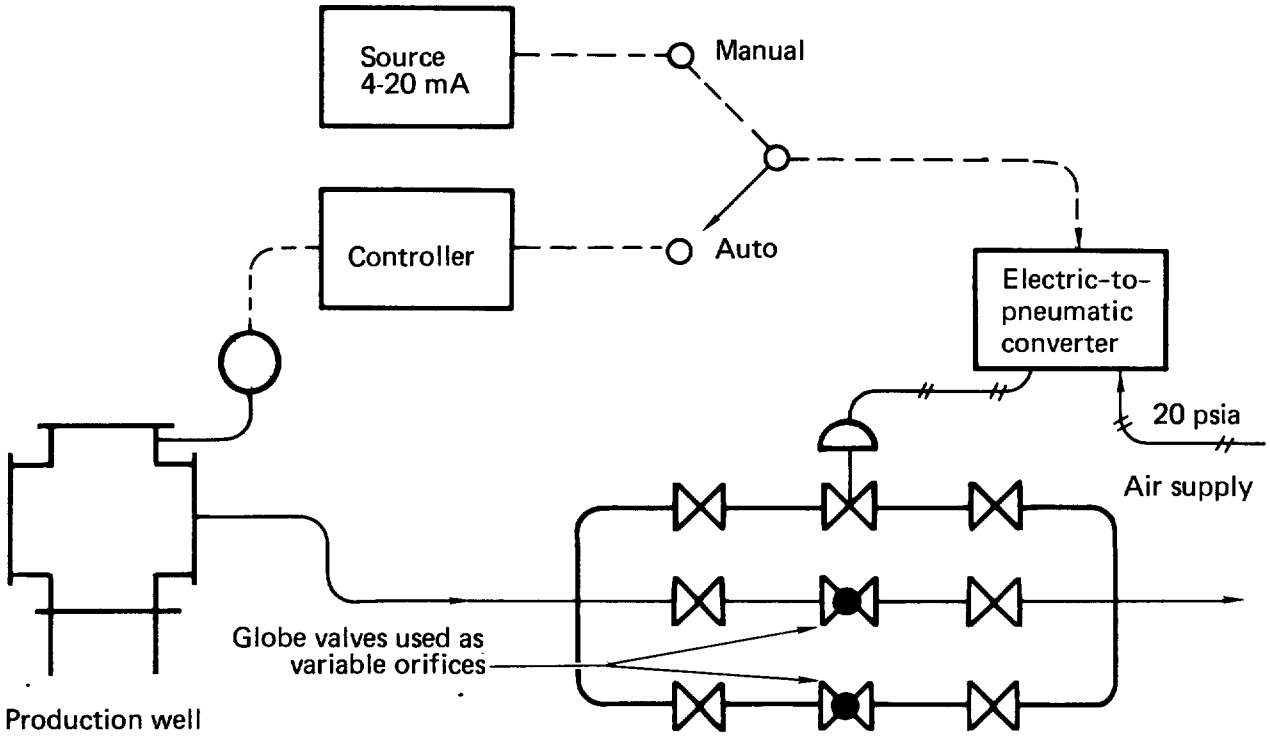

FIG. 6. Backpressure control system for Tono No. 1.

recorded in the control room. This signal, a transducer output of 4–20 mA, is fed into a controller. An electronic signal carrying a set-point adjustment goes from the controller to an electronic-to-pneumatic converter, which drives an air-actuated control valve, providing continuous pressure control on the system.

The pressure control valve is equipped with a manual override to permit manual operation. It is designed to provide a linear pressure response to the milliampere signal feeding the converter. The spring-loaded actuator will automatically close the valve upon loss of instrument air.

One of the major components contained in the exhaust system is the incinerator, also referred to as a low-level flare because the combustion of exhaust gases and entrained tars occurs in a combustion chamber at the base of a refractory-lined stack. The incinerator is 5-1/2 ft in diameter and 30 ft high. It is an induced-draft unit, with gas and combustion air introduced through nozzles around the base of the stack. Allowance is made for introducing additional combustion air by induced draft through supplementary nozzles equipped with closures below the gas nozzles.

Auxiliary components of the incinerator include a propane-fired pilot burner and igniter and additional nozzles for tar drainage and reinjection. Several thermocouples are positioned inside the refractory lining of the incinerator to monitor operating temperatures.

The incinerator is designed to handle a nominal throughput of 3000 scfm of exhaust gases of the quality (250 Btu/scf) expected during gasification. At gasification rates resulting from higher injection flows, the incinerator performance may become marginal since the exhaust flow rate will easily exceed 3000 scfm. Exceeding the capacity of the incinerator will result in either incomplete combustion of the produced gases or excessive temperatures inside the combustion chamber. The incinerator's operation will be monitored by continuously measuring its combustion chamber temperatures and testing its exhaust for evidence of hydrocarbon particles. Flow to the incinerator will be adjusted as required to maintain its operation within acceptable limits.

The incinerator is intended to be used for gas disposal during the early stages of gasification as well as during reverse combustion linking. During both of these phases, low quality gas and entrained wet coal particulates and tars represent the most difficult combustion processing. This unit is reasonably well equipped to handle this type of effluent because of its auxiliary burner and the large plenum located in its base.

At high gasification rates—for injection rates greater than 2000 scfm—the capacity of the incinerator is augmented by use of the elevated flare. The flare is designed to handle a maximum flow of 20,000 scfm of 125-Btu/scf gas. It is equipped with three propane-fired igniters and pilot burners to ignite and stabilize the flame. The flare is 20 inches in diameter and 30 feet high. Thermocouples located in the pilot burner tips indicate ignition as well as flame failure.

An auxiliary feature of the flare is the flame front generator. It is used to ignite the pilot burners, which in turn are used to stabilize the flame at the tip of the flare. The flame front generator mixes propane and air in controlled ratios and ignites the mixture downstream of the mixing chamber. Ignition is by a manually operated electrical discharge. The ignited gas-air mixture travels through heavy-walled piping to the main source of fuel outlet: in the case of the flare, to the the pilot burners at the flare tip; or, as an auxiliary use, to the incinerator pilot burner.

Exhaust Gas Sampling System

A continuous gas-sampling stream is withdrawn from the exhaust gas manifold at the orifice flow sections and routed to an analytical facility for on-line analysis. This auxiliary system is equipped with a liquid knockout section (refrigerant-cooled) and an adsorbent system. A bellows-seal compressor is used to transfer the treated gas to the analytical equipment for chemical analysis. Delivery of the gas sample flow is controlled at a maximum of 1 scfm and 5 psig at the facility.

A second gas-sample processing system, running in parallel with the system described above, is used to provide a gravimetric determination of water and tar content of the exhaust gas. Liquid knockout heat exchangers identical to those provided for the gas analysis stream remove water and tar and divert them to collection containers which will be periodically removed and weighed. Dry gas test meters are used to measure total throughput of the system during the sampling period. Pressure and temperature monitoring across

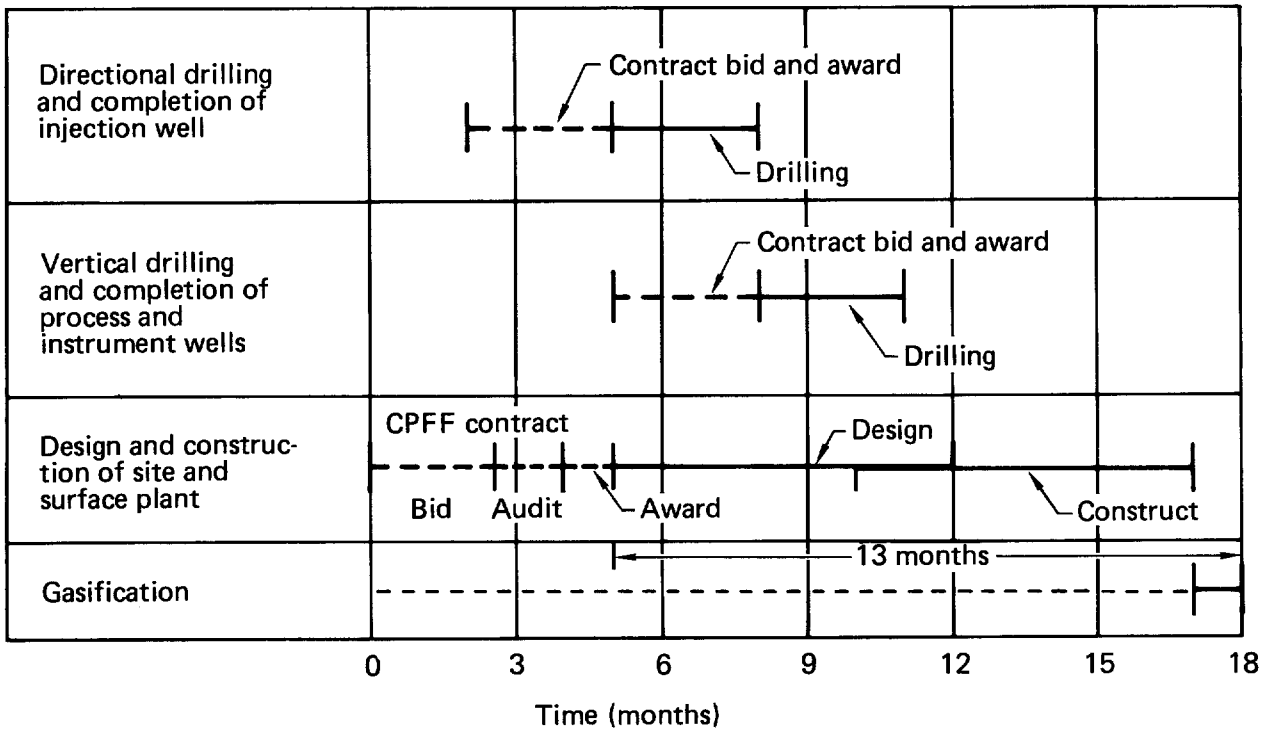

FIG. 7. Schedule for Tono No. 1.

TABLE 4. Estimated costs of the Tono No. 1 experiment (1982 dollars).

Directional drilling	550,000
Vertical drilling and instrumentation	600,000
Process well drilling and completion	150,000
Surface plant	2,000,000
30-day gasification run	800,000
Subtotal	4,100,000
Manpower and overhead costs, assuming five months additional for shutdown and monitoring	3,200,000
Total	$7,300,000

results obtained. In addition, at least two special briefings will be prepared for presentation to the Gas Research Institute, and two formal presentations will be given at appropriate symposia. It is expected that a reasonable number of briefings for other groups such as the Washington State participants will be required.

—R. W. Hill
C. B. Thorsness
D. S. Thompson
R. J. Cena
M. J. Shannon
D. R. Stephens

the test meter are provided to establish standard volumetric throughput and arrive at a determination of the total water and tar concentration of the exhaust gas. The flow rate of gas through this system is controlled to about 20 scfh.

The heat exchangers used in both of these systems are tube-and-shell type units with gas flowing on the tube side. Two of these heat exchangers operate in series in each system. The tube side of the exchangers is exposed to the receiving containers attached to the bottom of the units. Attachment of the receivers is designed for easy removal, to facilitate sample removal and cleaning of the internal surfaces of the tubes.

Water Systems

The auxiliary water systems associated with the experiment include seam-dewatering facilities, water-cooling provisions, and a waste-water disposal system.

Initial dewatering of the coal seam and discharge of water from the process wells during ignition, reverse burning, and the early (low-temperature) gasification phase are handled by water discharge lines located in the sumps of wells A and B. These lines are used as air-lift or gas-lift devices. They discharge water into a holdup tank where separated gas is vented to the incinerator and the water is reinjected into the coal seam as cooling water.

The water system also provides pressurized cooling water for the exhaust well in the event wellhead temperatures exceed safe limits.

A further function of the water system is to remove liquid accumulations from the base of the elevated flare and incinerator. These liquids are collected in the holdup tank. Collected tars are reinjected into the incinerator after separation in this tank. The waste water is discharged into the wells as cooling water.

SCHEDULE AND COSTS

About 13 months will be required to complete the basic experiment, from approval of the preliminary plan and complete funding, to completion and shutdown of the field operation (but not including time for permit acquisition, postburn coring, analysis, and reporting). This estimate assumes no unusual trouble in purchasing long-lead-time items or in acquiring the necessary permits. If any of the major secondary goals are funded, the time in the field will be increased.

A schedule giving an approximate task breakdown is shown in Fig. 7. The schedule assumes that the major contracts have been written and negotiated, and that the contractor personnel have been assigned. It also assumes that all permit requirements will be met before any construction is started. The site-characterization hydrology measurements and the large block tests should be completed before a final commitment is made. No time or funds are included for either of those activities or for any environmental work needed to monitor Tono No. 1. Total cost of the test, assuming only primary goals are funded, will be approximately $8 million. A breakdown of this estimate by category is given in Table 4.

Again, these costs do not include site characterization or environmental program costs. We would estimate at least $500,000 for each of these programs. Also, no allowance is made for other parallel programs, such as laboratory work, modeling, etc.

Each additional instrumentation well can be expected to cost $25,000 to $30,000, including contents and on-site manpower. The LATRAN system adds another $7,000 to $10,000 to this figure, depending on how many receiving wells are required. These costs do not include operating manpower, only installation.

Additional gasification time will cost about $27,000 per day including manpower and oxygen or air.

Since the experiment will take 13 months to complete, the earliest completion date possible is November 1982, assuming an October 1981 starting date. Hence the cost figures listed above allow for some inflation.

When the gasification experiment has been completed the fire will be extinguished and the burn zone allowed to cool. When the burn zone has cooled sufficiently, a postburn coring program will be needed to complete the diagnosis of the experiment. Since the cooling time is expected to be 6 to 12 months, the postburn coring should be considered separately. Hence no funds for it have been included in the estimates given here.

The reporting procedure for this test will be via our usual quarterly and monthly progress reports as well as published reports covering all aspects of the

MATHEMATICAL MODELING FOR LABORATORY COAL-BLOCK EXPERIMENTS

We have been developing a mathematical model for laboratory-scale coal-block experiments in order to improve our understanding of the physical and chemical processes governing the burning and growth of the cavity within the block. This model will later be adapted to larger scale coal-block experiments, and finally to full-scale field experiments. We hope to obtain scaling laws and other insights from the model.

At this point in our modeling we are considering the same chemical and physical phenomena as were treated in earlier models of gasification in a borehole. In order to maximize our physical insight, we have worked with the simplest models, which give the major qualitative features of the process. When we thoroughly understand these processes, we will add refinements that will lead to more accurate quantitative results.

In this report we examine the implications of a surface reaction rate that may be limited either by chemical kinetics or mass transport, depending on the temperature. A simple numerical model is described and its results are presented. The cavity shape is shown to depend upon assumptions about the gas flow in the borehole, so that a simple differential equation can give the approximate cavity shape. Finally, it appears that discrepancies between calculated and experimental cavity shapes are due to the assumption of plug flow in the model.

DEPENDENCE OF REACTION RATE ON CHEMICAL KINETIC AND MASS TRANSPORT RATES

For simplicity we consider only the burning of pure carbon—rather than coal, which contains moisture and hydrocarbons. This results in two major simplifications. First, only one chemical reaction need be considered,

$$2C + O_2 = 2CO \quad , \qquad (I)$$

which assumes that CO is the only product of carbon oxidation. Of course CO_2 could be included as a product, but its inclusion would have little effect on the temperature, because twice as much oxygen is needed, and the heat of reaction per unit mass of O_2 is actually somewhat smaller. The second simplification comes from the fact that the reaction is confined to the surface because the vapor pressure of carbon is so low that we need not consider gas-phase carbon.

This simplification restricts the model's applicability. The model provides a reasonable description of the burning of pure graphite, or charcoal, where one observes little or no flame in the gas phase. The model clearly ignores important aspects of the burning of wood or coal, where flames are quite conspicuous and have the effect of heating the solid by radiation. It might, however, model coal or wood burning in the case where flames have died down but the char remains hot and the solid continues to be consumed.

In our last progress report, surface temperatures were estimated by assuming that the reaction rate was limited by transport of oxygen from the gas stream to the solid surface. We now consider the case where the rate may be limited either by the chemical kinetic reaction rate, R_{ch}, or by the oxygen transport rate, gm_{O_2}, where g is the mass transport coefficient and m_{O_2} is the mass fraction of O_2. The two rates can be combined to give a total reaction rate, R. The units of R are chosen to give the mass consumption of O_2 per unit area per second.

$$R = \frac{1}{1/gm_{O_2} + 1/R_{ch}} = \frac{gm_{O_2}\, R_{ch}}{gm_{O_2} + R_{ch}} \quad . \qquad (1)$$

The chemical reaction rate, R_{ch}, will be large at high temperatures and small at low temperatures. Examining the second form in Eq. (1) we see that when R_{ch} is large it dominates the denominator so that R is approximately gm_{O_2}, the mass-transport-limited case. Similarly, when R_{ch} is small we have R approximately equal to R_{ch}, much smaller than in the mass-transport-limited case. The variation of R with temperature will have a shape similar to the S-shaped curve of Fig. 8, which will be considered shortly. The transition from low to high rates occurs at a temperature where R_{ch} becomes comparable in magnitude to gm_{O_2}.

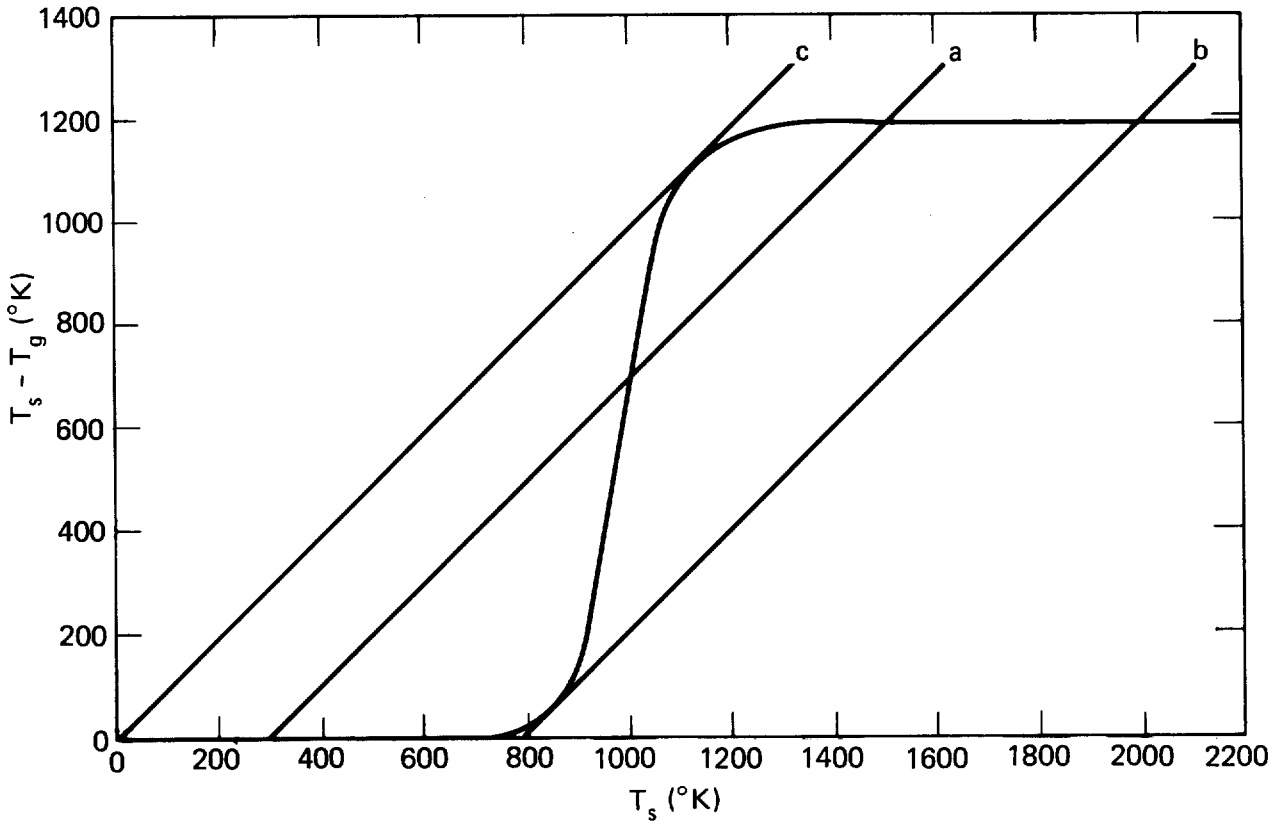

FIG. 8. Graphical representation of Eq. (5). The S-shaped curve represents the right-hand side of the equation, and the three parallel lines a, b, and c represent the left-hand side for three different values of T_g.

We can now derive an equation for the surface temperature of the solid using reaction rate R. Note that R is the rate at which O_2 arrives at the surface, as well as the reaction rate. This is obvious when R is limited by mass transfer. It is also true when R is limited by the chemical reaction rate because the flow of oxygen normal to the surface must just balance the consumption.

Calculating the mass balance is made easier if we define stoichiometric mass ratios, η_i, for each species i in reaction (I). Because other parameters are given in terms of unit mass of O_2, $\eta_{O_2} = 1$. Reaction mass balance requires

$$\eta_{O_2} + \eta_C + \eta_{CO} = 0 \quad . \tag{2}$$

Thus $\eta_C = 0.75$ and $\eta_{CO} = -1.75$, the negative denoting a product of the reaction.

To do mass and energy balances on the solid we define one boundary near the surface but an infinitesimal distance into the gas. The other boundary is located well inside the solid at a point where the properties, including temperature, are those of the unperturbed solid. As the surface is consumed and regresses at velocity v_s, the boundaries move with the same velocity. Mass crosses the interior boundary at a rate $v_s\rho_s$, where ρ_s is the density of the unperturbed solid. At the other boundary O_2 enters and CO exits at rates proportional to R, giving a mass balance.

$$v_s\rho_s = -R(\eta_{O_2} + \eta_{CO}) = \eta_C R \quad . \tag{3}$$

The second equality results from substituting Eq. (2).

Similar reasoning gives an enthalpy balance.

$$\begin{aligned} R\Delta H_r + v_s\rho_s C_s T_c + R\eta_{O_2} T_s C_{O_2}(T_s) \\ = -\eta_{CO} R\, T_s C_{CO}(T_s) \\ + gC_p(T_b)(T_s - T_g) \\ + \sigma(T_s^4 - \textstyle\sum \phi_k T_k^4) \quad . \end{aligned} \tag{4}$$

The first term on the left is the heat from the chemical reaction, with ΔH_r the enthalpy of reaction per unit mass of O_2 consumed. The second term is the enthalpy of the unperturbed solid entering the system, with C_s the specific heat of the solid, evaluated at the unperturbed solid's temperature, T_c. The first term on the right is the enthalpy carried by the CO gas leaving the system at the surface temperature, T_s. The negative sign is due to the negative value of η_{CO}. The specific heat of CO per unit mass at constant pressure, $C_{CO}(T_s)$, is evaluated at the surface temperature. The second term on the right is the heat transfer to the gas stream at temperature T_g. The specific heat $C_p(T_b)$, is evaluated for some appropriate composition in the boundary layer where the temperature is T_b. Different conventions for determining this point will give slightly different results. The last term is the heat lost by radiation to various surfaces at temperatures T_k with optical view factors ϕ_k. Radiative heat transfer to the gas can be included in the summation.

For simplicity, radiative heat transfer will be neglected in what follows. This would be a poor assumption if the reaction surface were near other, cold surfaces, but it is more reasonable in a borehole where the surrounding surfaces are at a comparable temperature. In that case the primary effect of radiation will be a slight smoothing of the temperature profile. This will have little effect on the reaction rate, which, as we will see below, depends only on the availability of oxygen—once the surface temperature exceeds the minimum temperature—to assure rapid chemical reaction. Similarly, radiative heat transfer to the gas in the borehole will be neglected, though it could enhance the heat transfer between the gas and the solid surface.

If we treat the gas temperature, T_g, as a parameter in Eq. (4) and use Eq. (3) to eliminate v_s, we get an equation for T_s.

$$T_s - T_g = \frac{R[\Delta H_r + \eta_c C_s T_c - C_{eff} T_g]}{gC_p(T_b) + RC_{eff}} \quad , (5)$$

where

$$C_{eff} = -\eta_{CO} C_{CO}(T_s) - \eta_{O_2} C_{O_2}(T_s) \quad .$$

Note that despite the minus signs C_{eff} is positive because η_{CO} is negative, and C_{eff} is approximately 0.7 C_{O_2}. The specific heats depend weakly on T_s, as does R, except in the transition region between low and high rates. Equation (5) is quite similar to, but not identical to, the expression for surface temperature given in the last quarterly report. The minor differences result from a more careful consideration of the enthalpy of the gases crossing the boundary in the present treatment.

To understand the implications of Eq. (5) it is helpful to make the further approximation that the molar specific heats are the same for all species and do not vary with temperature. Because the major gaseous species are diatomic, their molar specific heats should be very nearly the same, and even the molar specific heat of the solid should not be greatly different. The specific heats will in fact vary with temperature, but Eq. (5) mainly uses the ratios, which will not vary as much. Designating the specific heat per mole as C, we get

$$C = W_i C_i \quad , \quad (6)$$

which, when combined with Eq. (2) gives

$$\eta_i C_i = \nu_i C / W_{O_2} \quad . \quad (7)$$

Substituting this in Eq. (5) gives

$$T_s - T_g = \frac{\Delta H_r W_{O_2}/C + 2T_c - T_g}{1 + g/R} \quad . \quad (8)$$

(The approximation $W_{O_2} = W_{air}$ was made for the last term in the denominator.) Substituting R from Eq. (2) gives

$$T_s - T_g = \frac{T_m}{1 + gm_{O_2}/R_{ch}(1 + m_{O_2})} \quad , \quad (9)$$

with

$$T_m = \frac{m_{O_2}(\Delta H_r W_{O_2}/C + 2T_c - T_g)}{1 + m_{O_2}} \quad . \quad (10)$$

It is clear from examining Eq. (9) that T_m is the value of $T_s - T_g$ when the chemical reaction rate, R_{ch}, is large. When R_{ch} is small compared to gm_{O_2},

the temperature difference will be proportionally small.

The chemical kinetic reaction rate can be written

$$R_{ch} = A(m_{O_2}\rho/W_{O_2}) \exp(-\theta_A/T) \quad , \qquad (11)$$

where A is proportional to the collision frequency and can be adjusted for effects due to the solid, $m_{O_2}\rho/W_{O_2}$ is the concentration of O_2 (moles/unit volume), and θ_A is the activation temperature, i.e., E_a/R. Substituting this in Eq. (9) gives

$$T_s - T_g = \frac{T_m}{1 + \left[\dfrac{gW_{O_2} \exp(\theta_A/T_s)}{A\rho(1 + m_{O_2})}\right]} \cdot \qquad (12)$$

The gas temperature, T_g, can be considered to be a parameter, but Eq. (12) is a transcendental equation which cannot be solved directly for T_s. Instead, the two sides are plotted separately in Fig. 8, using the parameter values given in Table 5. The right-hand side is the S-shaped curve, and the left-hand side is represented by the diagonal lines, each having a different value of T_g, equal to the value of T_s where the line intersects the horizontal axis. The equality of Eq. (12) is satisfied when the diagonal lines intersect the S-shaped curve. Interestingly, the curve labeled "a" has three intersections which will be discussed shortly.

TABLE 5. Constants used in Eq. (12) to obtain Fig. 8.

Quantity	Value
A	3×10^6 m/s
θ_A	20,000 K
ρ	0.33 kg/m^3
ΔH_r	7.06×10^6 J/kg
W_{O_2}	0.032 kg/mol
C	30 J/mol·K
m_{O_2}	0.20
g	0.05 kg/m^2·s

Figure 8 was plotted holding T_m constant at 1188 K, the value when T_g is 1000 K. In reality T_m drops about 17 K per 100 K increase in T_g, as shown by Eq. (10). Thus, the single S-shaped curve should be replaced by a family of curves, one for each value of T_c. But this would add unnecessary complexity. The location of the steep portion of the curve is easily determined from Eq. (12). The value of $T_s - T_g$ is $T_m/2$ when the denominator of Eq. (12) is 2. This gives

$$\theta_A/T_s = \ln[A\rho(1 + m_{O_2})/gW_{O_2}] \quad , \qquad (13)$$

which has a given value of 20.4, yielding T_s = 981 K for the values of the constants given in Table 5. This is independent of T_g, so all curves of the family would make the transition to high temperature at the same point; the only difference would be the value of the maximum temperature.

We return now to the three intersections of diagonal line "a" with the S-shaped curve. Each represents a solution of Eq. (12). The solution on the steep part of the curve is physically unstable. Such a large value of $T_s - T_g$ would raise the gas temperature, moving the diagonal line to the right and lowering $T_s - T_g$. The stable steady-state solutions lie on the flat portions of the S-shaped curve.

Whether the solution for line "a" lies at large or small values of $T_s - T_g$ depends on the previous history of the system. If the system starts with both T_g and T_s near 300 K, the value of $T_s - T_g$ will remain small as T_g is increased until line "b" is reached. At that point there is only one solution, $T_s - T_g$ approximately equal to T_m. Further increases in T_g cause no change except for the small decrease in T_m noted above. Once the high temperature branch of the S-shaped curve has been reached, decreases in T_g have little effect until T_g is so low that line "c" is reached. The solution then jumps to the lower branch at a low value of T_g. In Fig. 8 this value is just above 0 K. This hysteresis corresponds to our experience. We must heat a piece of charcoal to high temperature to ignite it, corresponding to a large value of T_g. Once it is lit it will continue to burn in ambient air at about 300 K. To extinguish it we must remove the oxygen long enough for it to cool, or we must cool the surface with something like water. Equation (12) thus has considerable physical significance. Adding radiative

heat loss and other reactions can add bumps and wiggles to the S-shaped curve, and perhaps additional solutions, but the physical interpretation will change little.

We also note that the oxygen consumption rate, R, which determines the chemical heat release rate, is essentially bistable. For conditions where the surface temperature is well above the gas temperature, R is approximately equal to gm_{O_2}, the oxygen mass transport rate. When the surface and gas temperatures are nearly equal, R is negligible, except near the knee of the S-shaped curve where it is still only a fraction of gm_{O_2}.

Equations (5) and (12) do not permit a cold surface to cool the gas. Consider the situation near the exit of the coal block under conditions where virtually all of the oxygen has been consumed and the gas heated by the reactions. Initially the surface downstream will be cool and no reaction can occur because of the absence of oxygen. Intuitively, one expects the cooler surface to reduce the gas temperature, but negative values of $T_s - T_g$ are not allowed by Eq. (5) or (12). That is because they represent steady-state solutions, and after an infinite time the wall temperature will reach the gas temperature in the absence of chemical reactions. This situation occurs in numerical simulations of the coal block, where the block is divided into zones, and Eq. (5), along with a similar equation for the gas temperature, is solved in each zone. The calculated exit temperature is never less than the peak temperature elsewhere in the borehole. This is contradictory to experiments where the exit temperature is generally well below the peak.

The rigorous solution to this problem is to solve the partial differential equation for heat conduction into the coal, an approach that may be viable. An approximate treatment requires less computation but gives the correct qualitative behavior. Consider the situation where the coal is at a uniform temperature T_0. At time t_0 the gas temperature is suddenly increased to some value T_g greater than T_0. Heat will be conducted from the gas into the solid, resulting in temperature gradients in both. The gradient in the gas will be established in a second or so, but it will take minutes to establish the gradient in the solid. The rate of heat flow will be $k_s\,\partial T/\partial x$, where k_s is the thermal conductivity in the solid. Transient solutions to the heat conduction problem involve the function $\exp[-\Delta x^2/\alpha(t - t_0]$, so heat penetrates the solid to a depth Δx, equal to $(\alpha\Delta t)^{1/2}$, in time Δt. Using this Δx we can approximate the heat loss as

$$k_s\,\partial T/\partial x = (T_s - T_0)/\Delta x$$

$$= (T_s - T_0)(k_s\rho_s C_s/\Delta t)^{1/2} \qquad (14)$$

where the second equality is obtained using the definition $\alpha = k/\rho C$.

When the heat loss term of Eq. (14) is added to the right-hand side of the energy balance, Eq. (4), Eq. (5) is transformed to

$$T_s - T_g = \frac{A + B}{C} \quad , \qquad (15)$$

where

$$A = R(\Delta H_r + \eta_c C_s T_c - C_{eff} T_g) \quad ,$$

$$B = (T_0 - T_g)(k_s\rho_s C_s/\Delta t)^{1/2} \quad ,$$

$$C = gC_p(T_b) + RC_{eff} + (k_s\rho_s C_s/\Delta t)^{1/2} \quad .$$

When doing numerical calculations, we set T_0 equal to T_s at the beginning of a time step of length Δt and use Eq. (15) to obtain the new value of T_s. This procedure is not precise because the assumption of a uniform initial temperature distribution has been violated and the form chosen for the temperature gradient is not exact. However, it gives the proper steady-state solutions, the only errors occur during transient periods as the solutions approach steady state, and the duration of the transient is approximated fairly well. In addition, Eq. (15) allows transient periods when the solid surface is at a lower temperature than the gas, making possible calculated exit temperatures that are less than the peak gas temperature in the borehole, and allowing the surface downstream to heat slowly. After a very long time both the surface and gas temperatures downstream approach the peak temperature. If a more accurate solution is desired it is probably best to numerically solve the heat diffusion equation in the solid.

EQUATIONS FOR THE GAS

The simplest way to model the borehole is to assume plug flow of the gas with a boundary layer

between the gas stream and the solid surface. Plug flow implies that the velocity is independent of radial position and that the gas is of uniform composition; all gradients occur in the boundary layer. If this assumption is violated, the principal effect is in the mass and enthalpy balances, where the total inlet and outlet flows are considered. These balances involve integration over the inlet and outlet openings; if the velocity and compositions are nonuniform, these integrals give an effective radius which seldom differs from the true radius by more than 20 to 50%.

In deriving the mass and energy balances it seems natural to treat the boundary layer and plug flow regions as separate control volumes. However, so long as there are no chemical reactions in the boundary layer it contains no sources or sinks of mass or enthalpy, so it is simpler to treat the entire gas as a single control volume. Let us consider a short segment of the borehole with length Δz and radius r_1 at the inlet and r_2 at the outlet. (In this section subscript 1 will refer to inlet and subscript 2 to outlet. When it is also necessary to denote species, subscript i will be used, or the chemical name of the species.) The values of the input variables—temperature T_1, velocity u_1, density ρ_1, and mass fractions m_{i1}—are the outlet values of the next zone upstream, so can be assumed to be known. We need to find the output values of these same physical variables.

A separate mass balance can be done on each species. The outlet mass flow will equal the inlet plus the addition or reduction due to chemical reactions on the wall:

$$\pi r_2^2 u_2 m_{i2}\rho_2 = \pi r_1^2 u_1 m_{i1}\rho_1 - 2\pi r_a \Delta z \eta_i R, \quad (16)$$

where r_a is some average radius lying between r_1 and r_2, and the η_i are the mass stoichiometric coefficients for reaction (1). The minus sign occurs because of the sign convention used for the η_i. Note also that the solid carbon is not involved because only gas-phase species are considered.

The mass fractions, m_{i2}, and density, ρ_2, can be eliminated by using the ideal-gas equation of state, but in a less familiar form:

$$p/RT = \rho\sum(m_i/W_i) \quad . \quad (17)$$

Since flow velocities will be low and sections relatively short, little error is introduced by assuming constant pressure within a zone. If Eq. (16) for each species is divided by the appropriate molecular weight, W_i, and the sum over gas species is taken, substituting Eq. (17) gives

$$r_2^2 u_2 p/RT_2 = r_1^2 u_1 p/RT_1 - 2r_a \Delta z R(\eta_{O_2}/W_{O_2} + \eta_{CO}/W_{CO}). \quad (18)$$

This has eliminated $m_{i2}\rho_2$ but introduced T_2.

Setting the outlet enthalpy equal to the inlet enthalpy plus that which enters the gas from the solid wall gives

$$r_2^2 u_2 T_2 \rho_2 \sum m_{12} C_i(T_2) = r_1^2 u_1 T_1 \rho_1 \sum m_{i1} C_i(T_1) + 2r_a \Delta z \, [gC_p(T_b)(T_s - T_g) - RT_s \sum \eta_i C_i(T_s)]. \quad (19)$$

The only species involved in the last summation are CO and O_2, so the summation equals $-C_{eff}$, defined with Eq. (5). Substituting Eq. (16) in the left-hand side and rearranging, with T_g equal to $(T_1 + T_2)/2$, gives an equation for T_2.

$$T_2 = \frac{D + E}{F} \quad , \quad (20)$$

where

$$D = T_1(r_1^2 u_1 \rho_1 \sum m_{i1} C_i - r_a \Delta z g C_p) \, ,$$

$$E = 2T_s r_a \Delta z (gC_p + RC_{eff}),$$

$$F = [r_1^2 u_1 \rho_1 \sum m_{i1} C_i + r_a \Delta z (2RC_{eff} + gC_p)].$$

The C_i's in the numerator are evaluated at temperature T_1, and those in the denominator at temperature T_2. The specific heat in the boundary layer, C_p, is evaluated at temperature T_b, somewhere between T_g and T_s. Because some of the specific heats on the right-hand side of Eq. (20) depend on T_2, iteration is required for an exact solution. However, if $T_2 - T_1$ is reasonably small, as required for accurate numerical solution, little error is introduced

by evaluating all C_l at temperature T_l, which eliminates the need for iteration.

Once T_2 is known, the other outlet variables are easily obtained. Equation (18) gives u_2, and Eq. (16) then gives $m_{i2}\rho_2$, the sum of which is ρ_2, by definition.

A SIMPLE NUMERICAL MODEL

A simple numerical model for the burning of pure carbon in a borehole has been constructed using Eq. (15) with the gas equations described in the preceding section. To do this the length of the borehole was divided up into as many as 50 zones, each of length Δz_k. These zones need not be of equal length; indeed accuracy is improved if the lengths are adjusted so that the gas temperature change in each zone is roughly the same as in others. In each zone, Eq. (15) is solved iteratively to get the surface temperature of the solid. To get the value of T_g in Eq. (15), it is necessary to use Eq. (20) to calculate T_2, because $T_g = (T_2 + T_l)/2$. When the iteration has converged to satisfactory accuracy the other gas equations are used to calculate u_2, ρ_2, and m_{i2}, which are needed to calculate T_2 in the next zone downstream.

The iteration could be done by substituting a trial value of T_s, perhaps the value from the previous time step, in the right-hand side of Eq. (15) and calculating a new value of T_s. This new value is substituted on the right for the next iteration, and iteration continues until the value of T_s changes by less than some predetermined amount on each iteration. In practice a more efficient iteration procedure is used. An error function, $\epsilon(T_s)$, is defined equal to the difference between the left and right sides of Eq. (15). Convergence is achieved when ϵ approaches zero. The iteration procedure consists of calculating ϵ for two values of T_s and obtaining a slope, which is used to estimate the value of T_s that will give ϵ equal to zero. The new point is used to calculate a new slope until convergence is achieved. A standard, prepackaged subroutine was used for this purpose.

A potential problem arises from the fact that for some values of T_g there are three solutions of Eq. (5), which is the same as Eq. (15) but without the transient term. The iteration schemes mentioned in the previous paragraph will not converge to the solution on the steep part of the S-shaped curve, but will converge to either the high- or low-temperature solution, depending on the first trial value. To avoid numerical oscillation between these two solutions, the model first searches for solutions in the immediate vicinity of the previous value of T_s. When this search fails the range is extended to include both solutions. In practice this has worked well; transitions to high temperature occurred only when appropriate.

CALCULATIONS WITH THE NUMERICAL MODEL

The simple numerical model was used to calculate the cavity shape in a laboratory experiment where a 1-cm-diam hole was bored the length of a 0.61-m-long block of WIDCO coal. The gas flowing into the inlet was two-thirds steam and one-third oxygen (mole fractions), just hot enough to keep the steam from condensing. The flow rate vs time is shown in Fig. 9. The simple numerical model does not consider the steam-char reaction, so the steam was treated as if it were chemically inert. With this assumption the model was expected to underestimate the radius of the cavity, but not to give a qualitatively different cavity shape. We attempted to check this assumption with a similar calculation

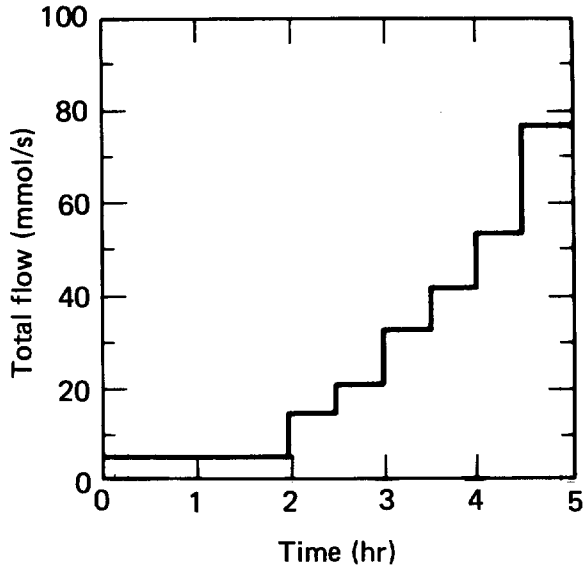

FIG. 9. Inlet flow schedule for the mixture of two-thirds steam and one-third oxygen (mole fractions) used in the laboratory burn experiments with small coal blocks.

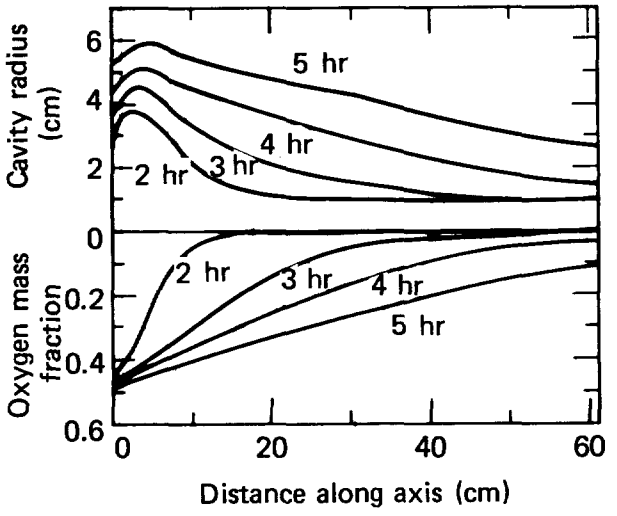

FIG. 10. Cavity shape and mass fraction of oxygen calculated with simple numerical model for flow schedule of Fig. 9.

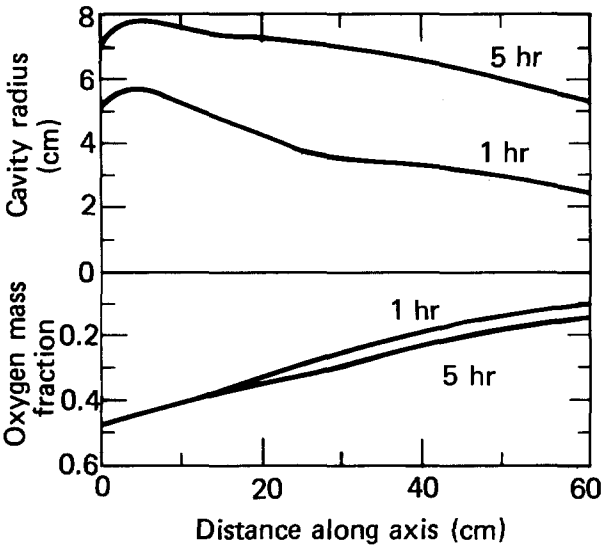

FIG. 11. Calculated cavity shape and mass fraction of oxygen for highest flow rate in Fig. 9 (78 mmol/s).

on another computer code which includes most of the chemistry (written by Prof. J. Riggs, West Virginia University, Morgantown, WV). Unfortunately, a numerical problem in the code distorted the cavity shape, but there was no indication that the additional chemistry caused a major difference in cavity shape.

Figure 10 shows the cavity shape calculated by the simple numerical model, along with the oxygen mass fractions. These are shown hourly, starting at 2 hr and ending at 5 hr, when the run was terminated. At 2 hr the cavity growth is all near the entrance of the borehole, while at 5 hr it is more equally distributed along the length, though it is still greater near the entrance. The profiles for oxygen mass fraction, m_{O_2}, are similar in shape.

The different shapes are due to the different flow rates, as illustrated by Figs. 11 and 12. Figure 11 shows the calculated cavity shape and oxygen mass fraction profile for the case where the burn is at the maximum flow rate for the entire 5 hours. Figure 12 shows the same data, but for the minimum flow rate. At the lower flow rate the cavity does not move downstream with increasing time, but continues to increase in radius for times up to 60 hours. At this time the total oxygen injected is the same as in 5 hours at the highest flow rate. The cavity volumes are approximately the

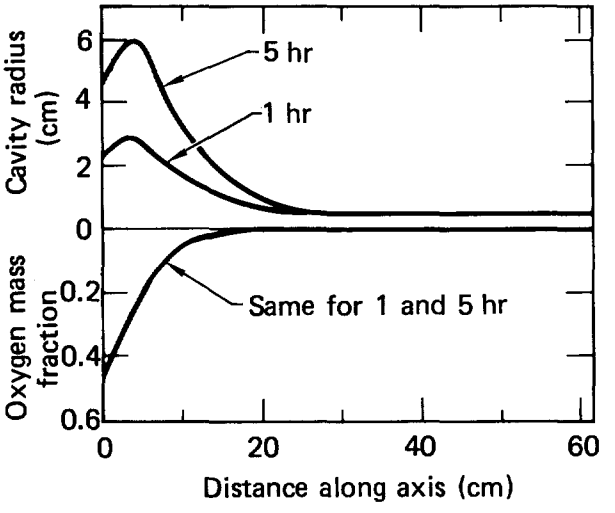

FIG. 12. Calculated cavity shape and mass fraction of oxygen for lowest flow rate in Fig. 9 (6 mmol/s).

same for the same total injected oxygen, as expected, since all or most of the oxygen reacts with carbon to form CO.

The calculated shape of the oxygen mass fraction profile is due to assumptions made about the gas flow. These assumptions influence the value of the mass transfer coefficient, g. For fully developed turbulent flow in a smooth pipe,

$$g = k\ Nu/2rC_p$$

and

$$Nu = 0.022\ Pr^{0.6}Re^{0.8} \quad , \tag{22}$$

where k is the thermal conductivity of the gas in the boundary layer, r is the radius of the pipe, Nu is the Nusselt number, Pr is the Prandtl number, and Re is the Reynolds number based on the pipe diameter. For air the Prandtl number is about 0.7, and we will neglect the small variation with temperature. If we let G be the total mass flow rate (kg/s) through the borehole,

$$G = \pi r^2 \rho u \quad , \tag{23}$$

then

$$Re = 2G/\mu\pi r \quad , \tag{24}$$

where μ is the dynamic viscosity of the gas.

Equation (22) is an empirical relation that gives the Nusselt number for fully turbulent flow, implying pipe Reynolds numbers of 2000 or greater. In modeling borehole combustion, Reynolds numbers as low as 30 were calculated at the lowest flow rates when the borehole had expanded to large radius. A flow with such a low Reynolds number is clearly laminar. The Nusselt number for laminar flow is 4.36, but Eq. (22) predicts a much lower value. To correct for this, the laminar Nusselt number was added to Eq. (22).

$$Nu = 4.36 + 0.017\ Re^{0.8} \quad . \tag{25}$$

This equation may overestimate the Nusselt number in the transition regime between laminar and turbulent flow, but this is probably a minor error compared to the assumptions made about the flow. Equation (22) is for fully developed turbulent flow in a smooth pipe of constant radius. We are considering a system where the flow in the inlet pipe is presumably turbulent but immediately expands into a region where the Reynolds number is well below the critical Reynolds number for the onset of turbulence. Furthermore, the radius of the borehole is changing rapidly and the surface is rough. It is unlikely that any textbook formula will give a more accurate expression for the Nusselt number.

We can obtain a differential equation for the change of m_{O_2} from Eq. (16) by letting Δz become so small that the inlet and outlet values of the other variables are aproximately equal. Substituting Eqs. (21), (24), and (25) gives

$$\frac{dm_{O_2}}{dz} = \frac{2\pi rg}{G} m_{O_2} = \frac{\pi k}{G}\left[4.36 + 0.017\left(\frac{2G}{\pi r\mu}\right)^{0.8}\right] m_{O_2} \quad . \tag{26}$$

The solution of this equation is

$$m_{O_2} = m_{O_2}(\text{inlet})\ \exp(-z/z_{O_2}) \quad , \tag{27}$$

with

$$z_{O_2} = \frac{G}{\pi k[4.36 + 0.017(2G/\pi r\mu)^{0.8}]} \quad , \tag{28}$$

where m_{O_2}(inlet) is the oxygen mass fraction at the inlet. The characteristic length, z_{O_2}, depends on the total mass flow rate, G. When the flow is laminar, z_{O_2} increases linearly with G; when the flow is fully turbulent, it increases as $G^{0.2}$. For the small coal block experiments, many of the flows will fall in the intermediate range where the dependence lies between these limits. For example, for the lowest flow in the experiment and calculation mentioned above, 6 mmol/s, the characteristic length would be 40 cm for a room-temperature value of k equal to 0.025 $J/m^3 \cdot s$. Examination of the printout shows that the numerical solution used a larger value of k, 0.12, because the calculated temperature was over 2000 K. This gives z_{O_2} equal to about 8 cm, essentially the value observed in Fig. 12. At the highest flow rates, 78 mmol/s, the Reynolds number is about 1000 and the denominator of Eq. (28) is twice as large as at low flow. The higher flow is 13 times larger, but z_{O_2} is only about seven times larger because of the larger denominator. This is confirmed by examining Fig. 11.

COMPARISON OF CALCULATION WITH EXPERIMENT

Figure 13 compares the predicted cavity shape of Fig. 10 with the observed cavity shape from a burn experiment with WIDCO coal. After the burn the block was cut in half, perpendicular to the borehole, as shown in Fig. 13. The outer contour is the cavity after the modified coal was removed by prying it loose with a screwdriver. In addition, a small amount of modified coal was shaken loose by vibration from the saw. This modified coal is assumed to be coal that was dried by heat from the surface chemical reaction. It had extensive cracks 1 to 5 mm in width and seemed to have about half the density of virgin coal. The contours shown in Fig. 13 should be considered approximate. The actual cavity was not quite symmetric, and the measurements were made with a ruler, so may not be precise. The inner surface was rather ragged, so the sketch must be considered to be an estimate.

The calculated cavity shape somewhat resembles the experimental shape in that the cavity gets narrower as the outlet is approached, but the differences seem more striking. First, the experimental volume is considerably larger. (It is hard to make a visual comparison from the figure because, in cylindrical geometry, regions farthest from the axis contribute the most to the volume.) This difference is due in part to the fact that the simple numerical model ignores the part of the cavity volume that results from removal of water and volatiles. Partial compensation for this omission could be accomplished by using a modified density in the numerical model. Some of the discrepancy in volume may be due to portions of the modified coal falling into the cavity and being consumed there. However, the amount of coal consumed should be proportional to the amount of oxygen injected, either as molecular oxygen or as oxygen contained in the injected steam. Any modified coal that was unburned should have been recovered when the block was cut open.

A second important difference between the calculation and the experiment is the shape of the cavity. The calculation shows the maximum radius near the entrance, followed by a profile which is close to an exponential decay. The experiment shows nearly constant radius throughout the first half of the borehole. In other block experiments we have seen cavities more nearly like a football in shape, though the flow rate and type of coal were different. For the calculation shown in Figs. 10 and 13, the inlet radius was allowed to increase, and all cavity growth was assumed to be radial. Another calculation, not shown, was done with the inlet

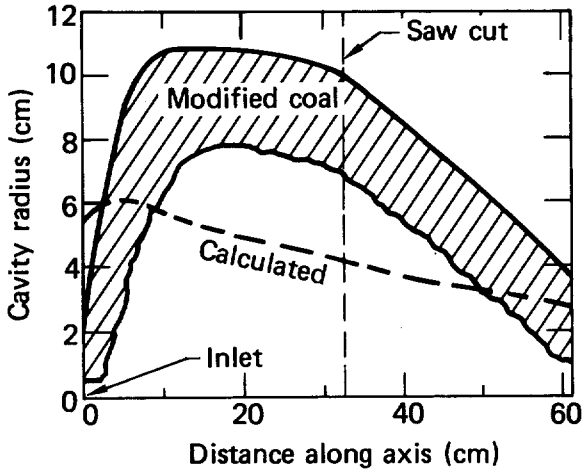

FIG. 13. Comparison of cavity shape calculated in Fig. 10 (at 5 hr) with cavity shape observed in a coal block subjected to a laboratory burn experiment. The flow schedule of Fig. 9 was used in both the calculation and the experiment.

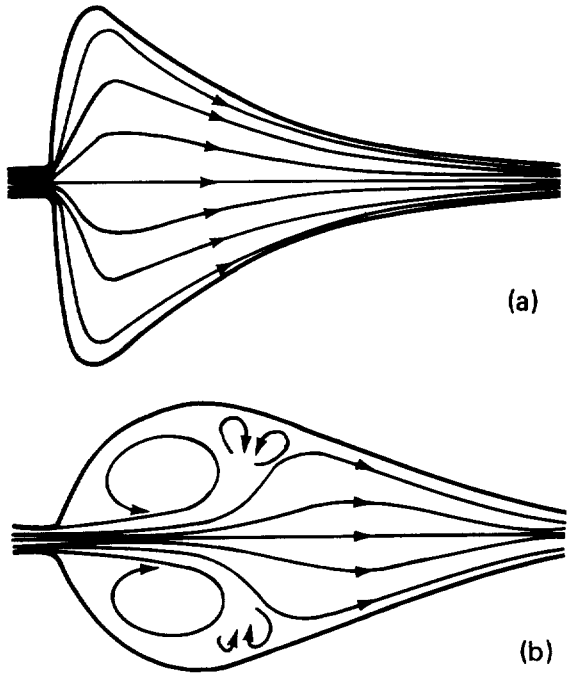

FIG. 14. (a) Plug flow assumption implies a simple and direct gas flow pattern in the cavity. (b) The actual gas flow pattern is probably much more complex, containing many eddies and vortexes.

radius fixed and cavity growth perpendicular to the surface at each time step. This increased the discrepancy between calculated and experimental cavity shapes. The maximum radius moved even closer to the inlet because most of the oxygen was consumed as the flow swept up the nearly vertical cavity face near the inlet. This discrepancy indicates that the model neglects some important aspect of the physics or chemistry.

The discrepancy is probably due to the plug flow assumption. Plug flow assumes streamlines similar to those sketched in Fig. 14(a). If the streamlines did in fact look like this, all of the oxygen would be consumed near the entrance unless the flow rate were high. A different flow pattern is shown in Fig. 14(b). In this case there are toroidal vortices, and the inlet gas first contacts the wall well downstream of the entrance. Thus the peak oxygen concentration will be well downstream and will decrease as one follows the streamlines adjacent to the walls. This would give a cavity shape similar to that of Fig. 14(b), which is merely a guess of the actual flow pattern, although it is based on known vortices which occur on the downstream sides of wedges and other flow restrictions. The smaller, counterrotating vortices have been added to minimize shears. Previous models of coal combustion with boreholes have not considered possible vortex formation and the attendant influence on cavity shape. We intend to concentrate on this problem in the next quarter.

—J. Creighton

GROUNDWATER CONTAMINATION MEASUREMENTS AT HOE CREEK NO. 3

The Hoe Creek No. 3 experiment, conducted during the fall of 1979, was located about 600 ft south of the Hoe Creek No. 1 site (see Fig. 15). It was the largest of the three UCG experiments carried out at Hoe Creek (see Table 6). On the basis of our previous experience in the area, we expected extensive roof collapse, gasification of both coal seams (Felix No. 1 as well as the lower-lying Felix No. 2, in which gasification was initiated), and interconnection of both coal aquifers and the overlying sand aquifer. We located our water-sampling wells in a pattern similar to that for Hoe Creek No. 2, except that we also drilled wells in the Felix No. 1 coal and the overlying sand before gasification (see Fig. 16). (Some pregasification coring results indicate that, at the Hoe Creek No. 3 site, the sand may lie directly on top of the Felix No. 1 coal, forming a single aquifer.) Well M-1 was drilled to monitor the transport of contaminants toward a spring located near Hoe Creek. The spring is about two to three thousand feet south of Hoe Creek No. 3, near the point at which one of the Felix coals outcrops. It may therefore represent a path from the groundwater system to the surface.

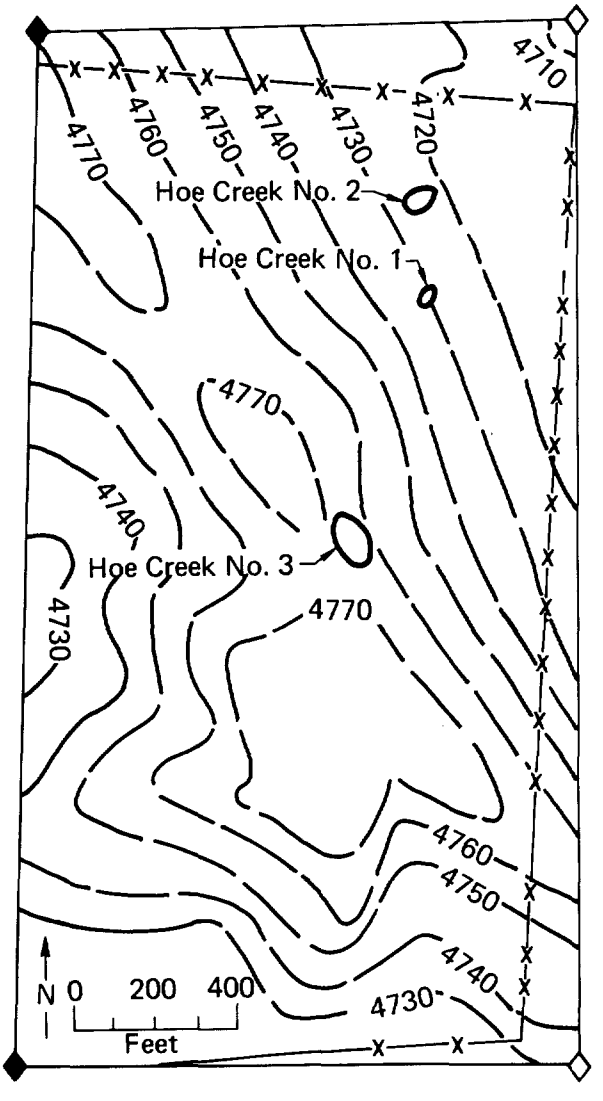

FIG. 15. Locations of LLNL's three UCG experiments at Hoe Creek in northeastern Wyoming. Contours are surface elevations.

During the Hoe Creek No. 2 experiment, some of the close-in water sampling wells were destroyed by the gasification process. We decided that, for the third experiment, we would not construct water wells close to the cavity until after gasification. An updated map of water well locations is shown in Fig. 17, and additional information is given in Table 7. Note that well W-2a (in Felix No. 1) was totally destroyed during gasification and does not appear on the updated map. Since we could not use well P-1, the injection well, to lower a pump to the bottom part of the cavity because of the rubble that had fallen into the cavity from above, we drilled well W-21, which was completed near the top of the Felix No. 2 coal inside the cavity.

PREGASIFICATION RESULTS

As indicated in Fig. 15, the site of Hoe Creek No. 3 is about 1000 ft from the other two UCG experiments in the area. We cannot be sure whether or not the water of all three aquifers at Hoe Creek No. 3 was affected by the two earlier experiments, especially by Hoe Creek No. 2. However, we believe that the effects, if any, were probably minimal. The pregasification concentrations of the major contaminant species in the groundwater obtained from the Felix No. 1 and No. 2 aquifers at the Hoe Creek No. 3 site were similar to the pregasification concentrations measured at the sites of the first two Hoe Creek experiments. Unfortunately, the only well in the sand aquifer, W-5b, contained no water before gasification. A comparison of baseline water quality (major contaminant species only) at Hoe

(Continued on p. 34)

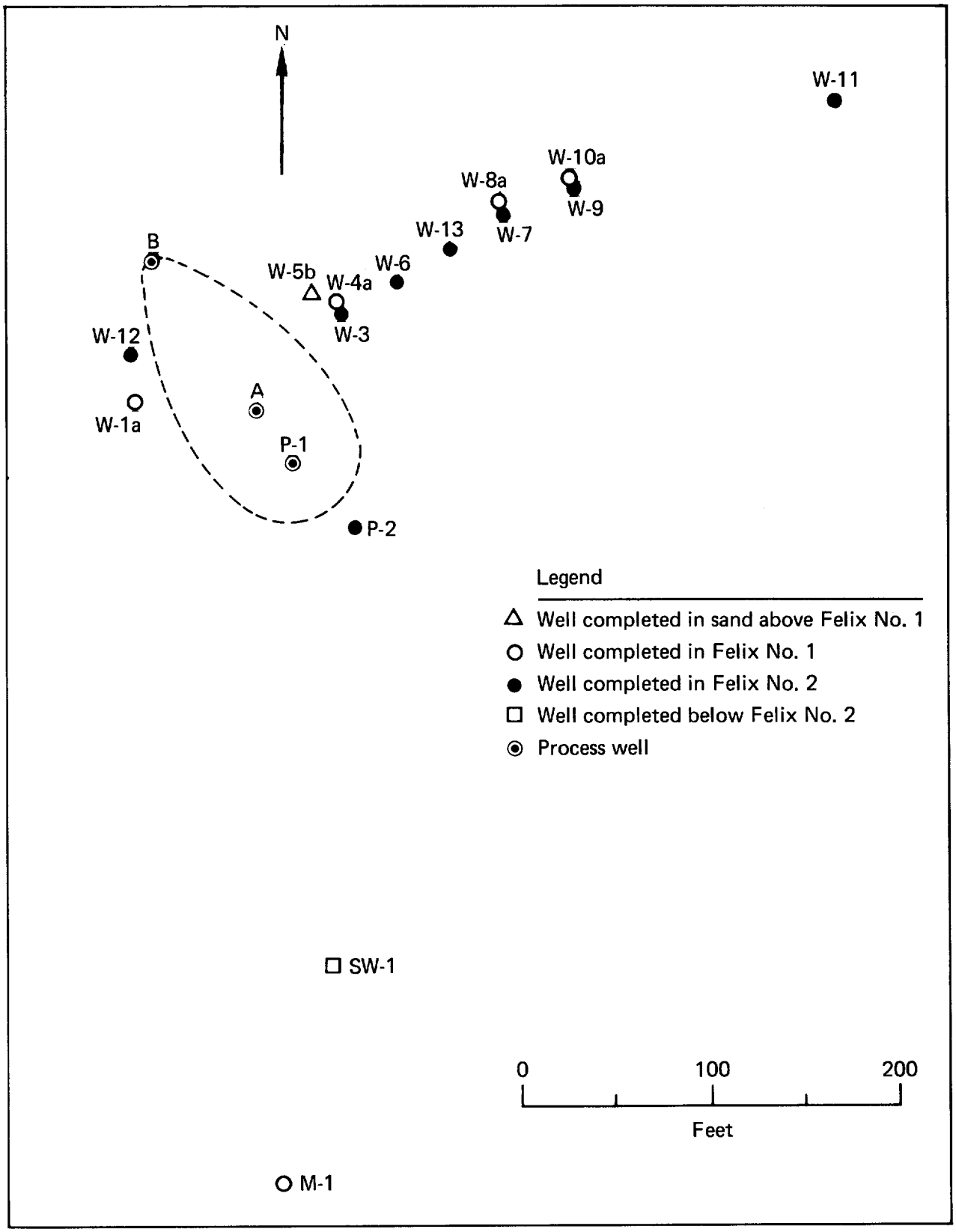

FIG. 16. Locations of the water sampling wells in the vicinity of Hoe Creek No. 3 that were completed before the gasification experiment. Additional wells drilled after gasification are included in the updated map of Fig. 17.

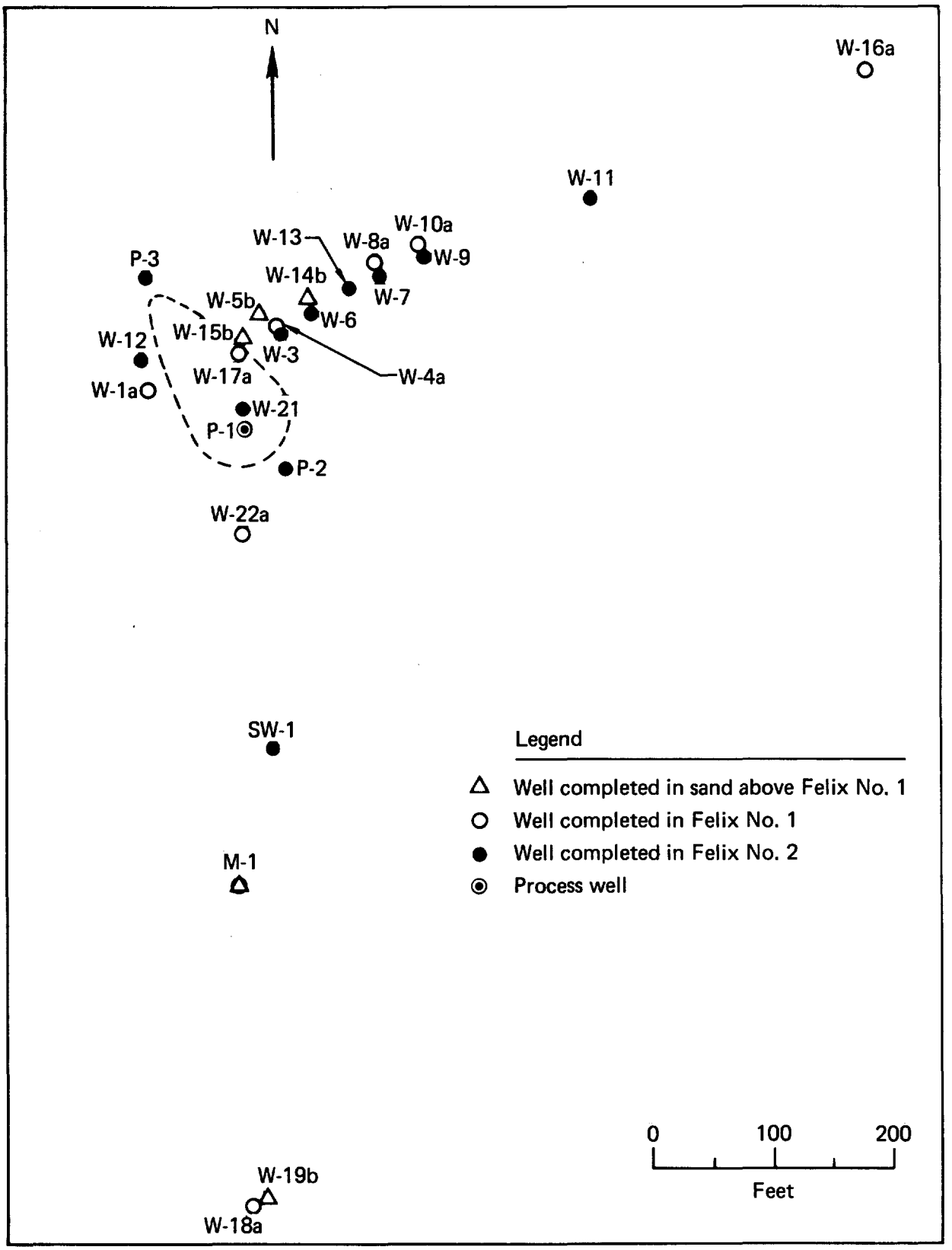

FIG. 17. Locations of all current water-sampling wells in the vicinity of Hoe Creek No. 3.

TABLE 6. Comparison of the three Hoe Creek experiments.

	Hoe Creek No. 1	Hoe Creek No. 2	Hoe Creek No. 3
Well separation (ft)[a]	33	60	130
Linking method	Explosive fracturing	Reverse combustion	Drilled hole plus reverse combustion
Coal gasified (tons)	130	2300	4200
System pressure (psia)[b]	30	47	43
Gas injected	Air	Air	Oxygen/steam
Gas loss (%)	7	20	14
Gasification period (days)	11	48	54
Overlying coal gasified?	No	Yes	Yes
Extensive roof collapse?	No	Yes	Yes
Surface subsidence?	No	No	Yes

[a]Distance between injection and production wells.

[b]Pressure maintained in cavity during gasification.

TABLE 7. Information on water wells in the vicinity of the Hoe Creek No. 3 site. All distances and bearings are with respect to the injection well P-1.

Well	Distance (ft)	Bearing	Date of completion	Aquifer
P-1	0	—	Pregasification	(Inside cavity)
P-2	48	N 50°E	Pregasification	Felix No. 2
W-1a	88	N 68°21′46″ W	Pregasification	Felix No. 1
W-3	85	N 20°2′55″ E	Pregasification	Felix No. 2
W-4a	90	N 16°52′26″ E	Pregasification	Felix No. 1
W-5b	92	N 9°4′52″ E	Pregasification	Sand
W-6	113	N 31°0′37″ E	Pregasification	Felix No. 2
W-7	177	N 41°11′54″ E	Pregasification	Felix No. 2
W-8a	178	N 39°1′59″ E	Pregasification	Felix No. 1
W-9	211	N 46°10′25″ E	Pregasification	Felix No. 2
W-10a	213	N 44°20′50″ E	Pregasification	Felix No. 1
W-11	350	N 56°41′46″ E	Pregasification	Felix No. 2
W-12	103	N 55°52′27″ W	Pregasification	Felix No. 2
W-13	145	N 37°30′37″ E	Pregasification	Felix No. 2
W-14b	119	N 28°E	November 1979	Sand
W-15b	69	N 1°52′34″ W	August 1980	Sand
W-16a	603	N 60°20′42″ E	October 1980	Felix No. 1
W-17a	66	N 1°52′34″ W	October 1980	Felix No. 1
W-18a	652	S 0°31′15″ E	October 1980	Felix No. 1
W-19b	646	S 1°10′21″ E	October 1980	Sand
W-21	13	N 10°15′30″ W	October 1980	(Inside cavity)
W-22a	102	S 1°56′ W	October 1980	Felix No. 1
M-1	384	S 0°56′42″ W	Pregasification	Felix No. 1/Sand
SW-1	288	S 5°6′35″ E	Pregasification	Below Felix No. 2

TABLE 8. Baseline data on groundwater quality for Hoe Creek No. 3 compared with the average of corresponding data for Hoe Creek Nos. 1 and 2.

	Felix No. 1 aquifer		Felix No. 2 aquifer	
	Hoe Creek No. 3	Hoe Creek Nos. 1, 2	Hoe Creek No. 3	Hoe Creek Nos. 1, 2
Electrical conductivity (μmho/cm)	2150	2070	1140	1080
pH	7.7	7.1	7.8	7.5
Temperature (°C)	11.1	10.5	11.8	11
Alkalinity (ppm)	362	260	396	401
Ammonium (ppm)	1.4	0.5	0.5	0.7
Boron (ppb)	57	50	63	86
Calcium (ppm)	140	190	34	36
Chloride (ppm)	7.7	8	43	13
Cyanide (ppb)	0	0	0	0
Magnesium (ppm)	34	73	7.8	10
Phenols (ppb)	0–2	0–2	0–2	0–2
Potassium (ppm)	8.7	8.0	5.1	5.4
Sodium (ppm)	375	190	250	214
Sulfate (ppm)	978	800	217	154

Creek No. 3 and the other two sites is shown in Table 8.

In October 1980, a year after Hoe Creek No. 3, we completed well M-2 in the sand aquifer above the Felix No. 1 coal. The well is located at the northwestern corner of the Hoe Creek site, more than 1000 ft from all three experiments. Judging from the CO_2 concentration (10 ppm) and the pH (7.7), we believe the measured concentrations of at least the major inorganic species, such as calcium, sodium, boron (as borates), etc., probably represent a good approximation to baseline conditions. However, we do detect phenols, and the concentration of dissolved organic carbon is higher than expected (as high as 10 ppm). Results of the analysis of water from M-2 are shown in Table 9.

TABLE 9. Groundwater quality data for well M-2, which was completed in the sand aquifer one year after the Hoe Creek No. 3 gasification experiment ended.

Temperature (°C)	10.0
pH	7.7
Electrical conductivity (μmho/cm)	2700
Ammonium (ppm)	1.4
Bicarbonate (ppm)	310
Boron (ppm)	80
Calcium (ppm)	270
Chloride (ppm)	9.3
Cyanide (ppb)	0
DOC[a] (ppm)	24
Magnesium (ppm)	67
Phenols (ppb)	19
Potassium (ppm)	16
Sodium (ppm)	320
Sulfate (ppm)	1300
Total sulfide (ppm)	0.8

[a]DOC is dissolved organic carbon.

POSTGASIFICATION RESULTS

Evidence began to accumulate during the gasification phase of Hoe Creek No. 3 that, as expected, roof collapse was extensive, both coal seams were gasified, and all three aquifers (the two coal seams and the overlying sand) were interconnected. We were unable to obtain groundwater samples

during the Hoe Creek No. 3 gasification, however, because all water wells were sealed to prevent gas leakage, which had been a problem during the Hoe Creek No. 2 gasification.

Following gasification, we initiated an extensive sampling program. We sampled the nearby groundwater six times during the first year, and in two subsequent operations have included sampling within the burn cavity. We have found that the relative levels of contamination in the three aquifers are similar to those for the second experiment: The sand aquifer is the least contaminated, and the Felix No. 1 coal aquifer is the most contaminated. A comparison of water quality data from the three aquifers at Hoe Creek No. 3, one year after gasification, is given in Table 10. Wells W-3 (in Felix No. 2), W-4a (Felix No. 1), and W-5b (sand) are all located about 90 ft from the injection well P-1.

Our data suggest that the Felix No. 2 coal aquifer at Hoe Creek No. 3 is much less contaminated after gasification than it was at Hoe Creek No. 2. A comparison of the water quality in two wells at about the same distance from the respective cavities is shown in Table 11. The differences in contaminant concentrations at the two sites may be explained by the following considerations:

1. The pregasification linking method at Hoe Creek No. 3 involved a directionally drilled horizontal hole connecting the injection and production wells in the Felix No. 2 coal. The horizontal linking hole ran about midway between the top and bottom of the seam. Postburn coring has shown that the coal below the linking hole was not gasified. By contrast, the entire thickness of the Felix No. 2 coal was gasified at Hoe Creek No. 2. At Hoe Creek No. 3, therefore, the Felix No. 2 coal formed a smaller fraction of the cavity surface than at Hoe Creek No. 2, and the density of pyrolysis products deposited in that surface would be expected to be correspondingly smaller. Furthermore, the sampling wells in the Felix No. 1 seam were completed in the lower half of the seam, so that water samples are drawn predominantly from the lower portion of the coal, which was less directly exposed to contamination.

TABLE 10. Comparison of groundwater quality data for the three aquifers at the Hoe Creek No. 3 site one year after gasification ended. Values in parentheses are baseline data.

	Felix No. 2 (well W-3)	Felix No. 1 (well W-4a)	Sand aquifer[a] (well W-5b)
Temperature (°C)	16.2 (10.3)	20.0 (11.0)	28 (10.0)
pH	8.3 (7.7)	6.4 (7.3)	6.1 (7.7)
Electrical conductivity (μmho/cm)	1750 (1850)	3400 (2600)	4000 (2700)
Ammonium (ppm)	0.59 (0.57)	3.5 (1.2)	4.8 (1.4)
Bicarbonate (ppm)	810 (410)	1700 (510)	1460 (310)
Boron (ppm)	80 (80)	120 (65)	190 (80)
Calcium (ppm)	58 (140)	320 (230)	440 (270)
Chloride (ppm)	39 (54)	5.8 (8.2)	6.5 (9.3)
Cyanide (ppb)	30 (0)	60 (0)	10 (0)
DOC (ppm)	9.7 (6.3)	35 (6.3)	33 (24)
Magnesium (ppm)	17 (14)	72 (40)	110 (67)
Phenols (ppb)	15 (3)	1600 (2)	0 (19)
Potassium (ppm)	11 (7.9)	15 (7.8)	24 (16)
Sodium (ppm)	370 (290)	540 (390)	620 (320)
Sulfate (ppm)	260 (220)	750 (980)	1600 (1300)
Total sulfide (ppm)	1.0 (0.6)	7.8 (0.9)	1.4 (0.8)

[a]The "baseline data" values here represent data from well M-2 one year after the Hoe Creek No. 3 experiment. Thus they cannot be considered true baseline data for the sand aquifer, but they should be close approximations to pregasification values, except for the DOC and the phenols.

TABLE 11. Change in groundwater quality in Felix No. 2 with time after gasification for Hoe Creek Nos. 2 and 3.

	Hoe Creek No. 3 (well P-2)				Hoe Creek No. 2 (well WS-6)			
Time (days)[a]	58	106	149	380	52	107	171	460
Electrical conductivity (μmho/cm)	3170	2000	2840	2600	2600	1950	1500	1400
pH	7.1	7.1	7.1	8.0	7.2	7.2	7.8	7.3
Temperature (°C)	12.7	23.4	31.2	25	13	15.9	18.7	23.5
Ammonium (ppm)	1.7	1.2	1.4	3.1	1.8	2.3	3.9	3.9
Boron (ppb)	110	100	140	120	230	290	370	310
Calcium (ppm)	300	220	160	46	170	110	69	55
Chloride (ppm)	33	34	36	36	12	13	10	13
Cyanide (ppb)	70	70	60	80	180	120	120	90
CO_2 (ppm)	233	193	137	7	103	74	17	—
Phenols (ppb)	230	420	240	8	2600	2500	800	370
Sulfate (ppm)	550	420	660	980	750	560	400	140
DOC (ppm)	45	52	32	6.3	—	—	27	10

[a]Time after end of gasification.

2. A slightly lower system pressure was employed during the Hoe Creek No. 3 gasification (Table 6), and we would therefore expect a lower concentration of pyrolysis products in the surrounding coal.

3. Some of our data suggest that there may be localized fracture systems in the coal seam, in addition to the normal porosity. Fluid flow through such cracks or fractures may be the dominant transport mechanism for both liquids and gases. If this effect is significant, it might explain apparent differences in the contaminant concentrations measured with two different sampling-well arrays. It would also have important implications for the design of a meaningful groundwater-monitoring plan for future gasification operations.

At Hoe Creek No. 2, we did not sample water from the Felix No. 1 coal aquifer until one year after gasification, and our initial sample from the sand aquifer was not obtained until two years after gasification. Therefore we cannot yet compare the results of water quality measurements in the sand aquifer at Hoe Creek No. 3 with corresponding data from the Hoe Creek No. 2 site. And only one such comparison for water quality in the Felix No. 1 coal is now possible. That comparison is shown in Table 12. Again, the Felix No. 1 aquifer

TABLE 12. Comparison of groundwater quality in Felix No. 1 one year after gasification at Hoe Creek Nos. 2 and 3.

	Hoe Creek No. 3 (well W-17a)	Hoe Creek No. 2 (well WS-10)
Distance to injection well (ft)	66	55
Temperature (°C)	50.0 (51.0)[a]	24.5 (35)[a]
pH	7.8	6.9
Electrical conductivity (μmho/cm)	3200	1700
Ammonium (ppm)	1.7	59
Bicarbonate (ppm)	430	1140
Boron (ppb)	2000	140
Calcium (ppm)	92	190
Chloride (ppm)	41	0.2
Cyanide (ppb)	160	230
DOC (ppm)	40	133
Magnesium (ppm)	100	53
Phenols (ppb)	13000	37000
Potassium (ppm)	86	9.2
Sodium (ppm)	520	130
Sulfate (ppm)	1400	0.4
Total sulfide (ppm)	33	28

[a]Numbers in parentheses are water temperatures in the respective cavities. These data suggest that well W-17a is probably closer to the boundary of the Hoe Creek No. 3 cavity than well WS-10 is to the boundary of the Hoe Creek No. 2 cavity.

seems less contaminated with pyrolysis products after gasification at the Hoe Creek No. 3 site than at the Hoe Creek No. 2 site. As suggested above, lower system pressure and directional differences may be important.

Because of the surface subsidence at Hoe Creek No. 3, it was dangerous for a time to get close to the injection well P-1. Therefore, we did not collect water from the Hoe Creek No. 3 gasification cavity until five months after the experiment. A comparison of the water quality inside the Hoe Creek No. 3 cavity with corresponding data from the Hoe Creek No. 2 cavity is shown in Table 13.

A comparison of cavity water quality from the first experiment, Hoe Creek No. 1, with that from Hoe Creek Nos. 2 and 3 shows very large differences. The water inside the cavities of the second and third experiments has had a much more complicated origin. It is made up of water from three aquifers with different water qualities and has been affected by the addition of large amounts of overburden material. The Hoe Creek No. 1 cavity water is mainly from the Felix No. 2 aquifer and was not affected by the addition of much overburden material.

Table 13 indicates that the concentrations of major inorganic species are much higher in the cavity water at Hoe Creek No. 3 than at Hoe Creek No. 2. This can perhaps be explained as follows: Throughout most of the Hoe Creek No. 3 experiment, oxygen was injected into the gasification zone at a point within or above the Felix No. 1 coal seam. Therefore more rock materials—located between the two coal seams—may have been exposed to heat at Hoe Creek No. 3 than at Hoe Creek No. 2. The temperature during gasification must also have been higher inside the Hoe Creek No. 3 cavity than in the Hoe Creek No. 2 cavity, because an oxygen-steam mixture was used for the third experiment whereas air was used for the second. Heat can change some insoluble minerals into soluble form. For example, insoluble $CaCO_3$ becomes soluble CaO. Furthermore, if some oxygen contacted these minerals, sulfides may have been turned into sulfate.

Water from well M-1, which was drilled to monitor contaminant movement toward the Hoe Creek spring, showed an increase in organic compounds when first sampled, soon after gasification. A plot of the changes in phenol concentrations in

TABLE 13. Change in cavity groundwater quality with time after gasification for Hoe Creek Nos. 2 and 3.

	Hoe Creek No. 2 (well A)				Hoe Creek No. 3 (well P-1)		
Time (days)[a]	106	170	271	452	149	201	380
Temperature (°C)	38	42	37	33	59	67	51
pH	8.6	8.5	8.8	8.8	7.5	8.0	8.6
Electrical conductivity (μmho/cm)	1800	1800	1450	1220	4960	4100	4000
Ammonium (ppm)	37	33	28	26	28	23	1.7(?)
Bicarbonate (ppm)	160	176	160	244	80	76	28
Boron (ppb)	2200	2200	2300	3100	4400	4300	3500
Calcium (ppm)	75	62	41	19	240	310	250
Chloride (ppm)	16	59	23	17	95	75	59
Cyanide (ppb)	140	80	30	90	74	119	120
DOC (ppm)	—	5.8	25	3.7	15	7.4	18
Magnesium (ppm)	15	13	11	6.5	75	75	59
Phenols (ppb)	750	360	330	82	40	60	67
Potassium (ppm)	85	79	64	46	120	110	110
Sodium (ppm)	250	240	220	180	720	610	532
Sulfate (ppm)	760	630	600	280	2200	2200	2000
Total sulfide (ppm)	42	6	40	57	1	0.5	0.2
Dissolved solids (ppm)	1290	1260	—	782	3400	3340	3050

[a]Time after end of gasification.

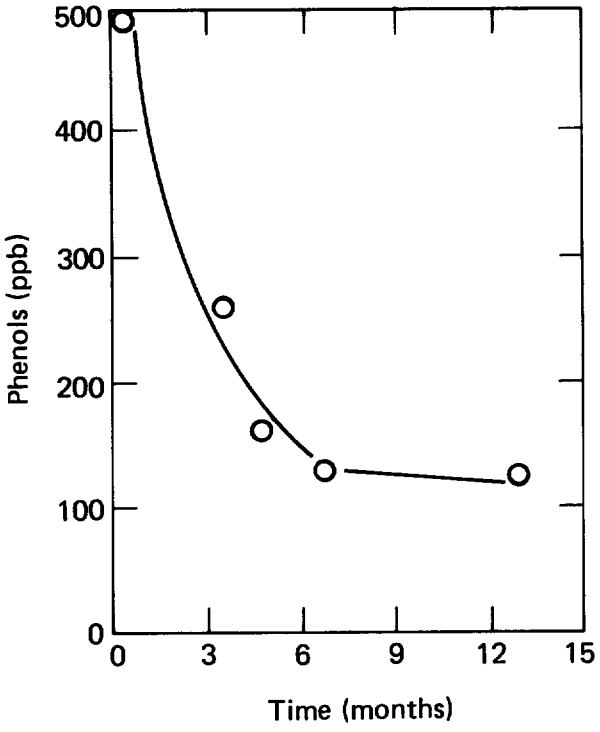

FIG. 18. Changing phenol concentration with time in well M-1, between Hoe Creek No. 3 and the Hoe Creek spring.

the water from M-1 is shown in Fig. 18. In order to obtain further information concerning the extent of phenol migration, we have drilled two additional wells between M-1 and the spring (one in Felix No. 1 and one in sand). Water quality data from these wells are not yet available.

At the end of the gasification phase at Hoe Creek No. 3, the groundwater reentered the hot gasification cavity and some of the resultant steam was vented to the surface. We collected a sample of the steam for analysis, but under conditions that did not guarantee a completely representative sample. Our sample contained about 2 ppm phenols, 1.5 ppm heterocyclic amines, and 0.5 ppm polycyclic aromatic hydrocarbons. We propose to obtain representative samples, if feasible, following future gasification experiments, to conduct more complete analyses, and to give added consideration to possible environmental implications of this aspect of the overall operation.

—F. T. Wang and S. W. Mead

REFERENCES

1. L. C. Bartel, T. C. Dobecki, S. L. Love, and B. E. Bader (Sandia National Laboratories, Albuquerque), and R. Stone, M. Adamson, and K. Tonnessen (Lawrence Livermore National Laboratory), *Site Selection and Characterization for an Underground Coal Gasification Test in Washington State*, draft report (1981).
2. M. J. Shannon, R. W. Hill, C. B. Thorsness, D. Thompson, and D. Skinner, "Early Cavity Growth in Forward Gasification," *Proc. Sixth Underground Coal Conversion Symposium* (Shangri-La, Afton, Oklahoma, July 13–17, 1980), CONF-800716 (1980), p. IV-92. Available from National Technical Information Service.
3. W. R. Aiman, R. W. Lyczkowski, C. B. Thorsness, and R. J. Cena, "Reverse Combustion in a Horizontally Bored Coal Channel," presented at Fifth Underground Coal Conversion Symposium, Alexandria, Virginia, June 18–21, 1979. See UCRL-82505 Preprint (1979).
4. R. W. Hill, C. B. Thorsness, D. S. Thompson, R. J. Cena, M. J. Shannon, and D. R. Stephens, *Large Block Tests—Experimental Plan*, Lawrence Livermore National Laboratory, Livermore, Calif., UCID-18944 (Feb. 25, 1981).
5. C. B. Thorsness, R. J. Cena, W. R. Aiman, R. W. Hill, and D. R. Stephens,"Hoe Creek No. 2: Underground Coal Gasification Experiment with Air and Oxygen/Steam Injection Periods," presented at 53rd Annual Fall Technical Conference and Exhibition of the Society of Petroleum Engineers of AIME, Houston, Texas, October 1–3, 1978. See also UCRL-80921 Preprint (1978).
6. R. W. Hill, C. B. Thorsness, R. J. Cena, W. R. Aiman, and D. R. Stephens,"Results from the Third LLL Underground Coal Gasification Experiment at Hoe Creek," *Proc. Sixth Underground Coal Conversion Symposium*, CONF-800716 (1980), p. I-19.
7. E. F. Laine and J. T. Okada, *Locating a Horizontal Borehole in the Earth Using High-Frequency Electromagnetic Probing from Vertical Boreholes*, Lawrence Livermore National Laboratory, Livermore, Calif., UCRL-82304 Preprint (August 1, 1979).
8. L. J. Katz, "Drill Bit Location, Guidance by Seismic Seen Feasible," *Oil and Gas Journal* (July 28, 1980), p. 197.
9. R. W. Hill and M. J. Shannon, *The Controlled Retracting Injection Point (CRIP) System for In Situ Coal Gasification*, Lawrence Livermore National Laboratory, Livermore, Calif., UCRL-85852 Preprint (1981, to be published).
10. R. W. Hill, *Burn Cavity Growth During the Hoe Creek No. 3 Underground Coal Gasification Experiment*, Lawrence Livermore National Laboratory, Livermore, Calif., UCRL-85173 Preprint (1981, to be published).
11. T. W. H. Caffey and D. E. Barnes, "A Buried Telemetry System for Temperature Measurements," *Proc. Sixth Underground Coal Conversion Symposium*, CONF-800716 (1980), p. VII-9.
12. C. B. Thorsness, "Model Calculations of the Hoe Creek Experiments," *LLNL Underground Coal Gasification Project Quarterly Progress Report—July through September 1980*, D. U. Olness, Ed., Lawrence Livermore National Laboratory, Livermore, Calif., UCRL-50026-80-3 (1980), p. 9.

WEC

U.S. Government Printing Office: 1981/9-789-002/5599